

Detection of Change Points in Piecewise Polynomial Signals Using Trend Filtering

Reza Valiollahi Mehrizi¹ and Shojaeddin Chenouri¹

¹Department of Statistics and Actuarial Science, University of Waterloo

Abstract

While many approaches have been proposed for discovering abrupt changes in piecewise constant signals, few methods are available to capture these changes in piecewise polynomial signals. In this paper, we propose a change point detection method, PRUTF, based on trend filtering. By providing a comprehensive dual solution path for trend filtering, PRUTF allows us to discover change points of the underlying signal for either a given value of the regularization parameter or a specific number of steps of the algorithm. We demonstrate that the dual solution path constitutes a Gaussian bridge process that enables us to derive an exact and efficient stopping rule for terminating the search algorithm. We also prove that the estimates produced by this algorithm are asymptotically consistent in pattern recovery. This result holds even in the case of staircases (consecutive change points of the same sign) in the signal. Finally, we investigate the performance of our proposed method for various signals and then compare its performance against some state-of-the-art methods in the context of change point detection. We apply our method to three real-world datasets including the UK House Price Index (HPI), the GISS surface Temperature Analysis (GISTEMP) and the Coronavirus disease (COVID-19) pandemic.

KEYWORDS: Change point detection, Trend filtering, Gaussian bridge process, Pattern recovery, COVID-19.

1 Introduction

The problem of change point detection is more than sixty years old. It was first studied by [Page \(1954, 1955\)](#), and since then, has been of interest to many scientists including statisticians. Many of the earlier developments concerned the existence of at most one change point; however, considerable attention in recent years has been given to multiple change point analysis, which has found applications in many fields such as finance and econometrics, [Bai and Perron \(2003\)](#); [Hansen \(2001\)](#), bioinformatics and genomics, [Futschik et al. \(2014\)](#); [Lavielle \(2005\)](#), climatology, [Liu et al. \(2010\)](#); [Pezzatti et al. \(2013\)](#), and technology, [Siris and Papagalou \(2004\)](#); [Oudre et al. \(2011\)](#); [Lung-Yut-Fong et al. \(2012\)](#); [Ranganathan \(2012\)](#); [Galceran et al. \(2017\)](#). Consequently, there is a vast and rich literature on the subject. In the following, we only review a body of literature on a retrospective change point framework closely related to our work and refer the

interested readers to [Eckley et al. \(2011\)](#); [Lee \(2010\)](#); [Horváth and Rice \(2014\)](#); [Truong et al. \(2018\)](#) for more comprehensive reviews.

We consider the univariate signal plus noise model

$$y_i = f_i + \varepsilon_i, \quad i = 1, \dots, n, \quad (1)$$

where $f_i = f(i/n)$ is a deterministic and unknown signal with equally spaced input points over the interval $[0, 1]$. The error terms $\varepsilon_1, \dots, \varepsilon_n$ are assumed to be independently and identically distributed Gaussian random variables with mean zero and finite variance σ^2 . We assume that $f(\cdot)$ undergoes J_0 unknown and distinct changes at point fractions $0 = \omega_0 < \omega_1 < \dots < \omega_{J_0} < \omega_{J_0+1} = 1$, where the number of change point fractions, J_0 can grow with the sample size n . Additionally, we assume that $f(\cdot)$ is a piecewise polynomial function of order $r \in \mathbb{N}$. These assumptions imply that, associated with $\omega_0, \dots, \omega_{J_0+1}$, there are change points locations $0 = \tau_0 < \tau_1 < \dots < \tau_{J_0} < \tau_{J_0+1} = n$, which partition the entire signal $\mathbf{f} = (f_1, \dots, f_n)$ into $J_0 + 1$ segments. More specifically, any subsignal of \mathbf{f} within segments created by the change points follows an r -degree polynomial structure with or without a continuity constraint at the change points. For more detail, see [Figure 2](#). Change in the level of a piecewise constant signal, known as the canonical multiple change point problem, and change in the slope of a piecewise linear signal are examples of the problem under consideration in this paper. In change point analysis, the objective is to estimate the number of change points, J_0 , as well as their locations $\boldsymbol{\tau} = \{\tau_1, \dots, \tau_{J_0}\}$ based on the observations $\mathbf{y} = (y_1, \dots, y_n)$.

The canonical multiple change point problem, where the signal \mathbf{f} is modelled as a piecewise constant function, has been extensively studied in the literature. In this framework, there are many approaches and we only attempt to list a selection of them here. The majority of these techniques seek to identify all change points at once by solving an optimization problem consisting of a loss function, often the negative log-likelihood, and a penalty criterion. [Yao \(1988\)](#); [Yao and Au \(1989\)](#) used the square error loss along with the Schwarz Information Criterion (SIC) as a penalty function to consistently estimate the bounded number of change points and their locations for the data drawn from a Gaussian distribution. Within the same setting, incorporation of various penalty functions including Modified Information Criterion (MIC) [Pan and Chen \(2006\)](#), modified Bayesian Information Criterion (mBIC) [Zhang and Siegmund \(2007\)](#), Simultaneous Information Theoretic Criterion (SITC) [Wu \(2008\)](#) and modified SIC [Ciuperca \(2011, 2014\)](#), have been studied. Specific algorithms such as Optimal Partitioning [Auger and Lawrence \(1989\)](#), Segment Neighbourhood [Jackson et al. \(2005\)](#), and pruning approaches such as PELT [Killick et al. \(2012\)](#) and PDPa [Rigaill \(2015\)](#) are developed to solve such optimization problems.

Apart from penalty-based techniques, another frequently used class of change point detection approaches encompasses the greedy search procedures in which they search sequentially for one single change point at a time. The most popular methods in this class are Binary Segmentation [Vostrikova \(1981\)](#) and its variants such as Circular Binary Segmentation (CBS) [Olshen et al. \(2004\)](#), and Wild Binary Segmentation (WBS) [Fryzlewicz et al. \(2014\)](#). In recent years, researchers have attempted to improve Binary Segmentation's performance from statisti-

cal and computational viewpoints. [Fryzlewicz et al. \(2018\)](#) suggested a backward (bottom-up) mechanism, called Tail Greedy Unbalanced Haar (TGUH), which is computationally fast and statistically consistent in estimating both the number and the locations of change points. Also, [Fryzlewicz \(2018\)](#) introduced Wild Binary Segmentation 2 (WBS2) to deal with the shortcomings of WBS in datasets with frequent changes. It has been shown that the method is fast in run time and accurate in detection.

Beyond the canonical change point problem, signals in which f is modelled as a piecewise polynomial of order $r \geq 1$ have attracted less attention in the literature despite many applications. For instance, piecewise linear signals are applied in monitoring patient health ([Aminikhanghahi and Cook \(2017\)](#), [Stasinopoulos and Rigby \(1992\)](#)), climate change ([Robbins et al. \(2011\)](#)), and finance ([Bianchi et al. \(1999\)](#)). In such a framework, [Bai \(1997\)](#) introduced a method based on Wald-type sequential tests, and [Maidstone et al. \(2017\)](#) devised a dynamic programming applied to an ℓ_0 -penalized least square procedure. In continuous piecewise linear models, [Kim et al. \(2009\)](#) developed a methodology called ℓ_1 -trend filtering. Furthermore, [Baranowski et al. \(2019\)](#) put forward the method of Narrowest Over Threshold (NOT), and [Anastasiou and Fryzlewicz \(2019\)](#) developed an approach called Isolate-Detect (ID) which both provide asymptotically consistent estimators of the number and locations of change points.

Our goal in this paper is to introduce a unifying method covering the canonical change point problem and beyond. More precisely, the method is cable of detecting change points in piecewise polynomial signals of order r ($r = 0, 1, 2, \dots$) with and without continuity constraint at the locations of change points.

The detection of change points in a sequence of data can be formulated as a penalized regression fitting problem. According to our notation, the quantity $f_\tau - f_{\tau+1}$ is nonzero if the signal f undergoes a change at point τ , and is zero otherwise. Moreover, if we assume that change points are sparse, that is, the number of locations where f changes, J_0 , is much smaller than the number of observations n , change points can be estimated using the one-dimensional fused lasso problem

$$\min_{\mathbf{f} \in \mathbb{R}^n} \frac{1}{2} \|\mathbf{y} - \mathbf{f}\|_2^2 + \lambda \sum_{i=1}^{n-1} |f_{i+1} - f_i|,$$

where $\mathbf{f} = (f_1, \dots, f_n)$.

This formulation of the canonical change point problem was first considered in [Huang et al. \(2005\)](#) and was applied to analyze a DNA copy number dataset. [Harchaoui and Lévy-Leduc \(2010\)](#) considered the same formulation and proved the consistency of the respective change point estimates when the number of change points is bounded. Employing sparse fused lasso which is composed of both the ℓ_1 -norm and the total variation seminorm penalties, [Rinaldo et al. \(2009\)](#) proposed a sparse piecewise constant fit and established the consistency of the corresponding estimates when the variance of the noise terms vanishes, and the minimum magnitude of jumps is bounded from below. However, [Rojas and Wahlberg \(2014\)](#) argued that the consistency results achieved by [Rinaldo et al. \(2009\)](#) are incorrect when a frequently viewed pattern, called *staircase*, exists in the signal. The staircase phenomenon occurs in a piecewise constant model when there are either two consecutive downward jumps or upward jumps in its

mean structure. The staircase pattern will be discussed in more detail in Section 6. Additionally, Qian and Jia (2016) showed that the lasso problem of Tibshirani (1996) when derived by transforming fused lasso does not satisfy the Irrepresentable Condition (Zhao and Yu (2006)) that is necessary and sufficient for exact pattern recovery. In particular, Qian and Jia (2016) proposed an approach called preconditioned fused lasso based on the puffer transformation of Jia et al. (2015) and established that it can recover the exact pattern with probability approaching one.

A similar approach to that of the piecewise constant signals can be considered for estimating change points in piecewise polynomial signals. In particular, a positive integer τ is a change location in an r -th degree piecewise polynomial signal f if τ -th element of the vector $\mathbf{D}^{(r+1)} \mathbf{f}$ is non-zero, denoted by $[\mathbf{D}^{(r+1)} \mathbf{f}]_\tau \neq 0$. Here $\mathbf{D}^{(r+1)}$ is a penalty matrix that will be defined in Section 2.2. Hence, change points can be estimated from nonzero elements of $\mathbf{D}^{(r+1)} \hat{\mathbf{f}}$, where $\hat{\mathbf{f}}$ is the solution of

$$\min_{\mathbf{f} \in \mathbb{R}^n} \frac{1}{2} \|\mathbf{y} - \mathbf{f}\|_2^2 + \lambda \|\mathbf{D}^{(r+1)} \mathbf{f}\|_1. \quad (2)$$

The aforementioned problem was first studied by Steidl et al. (2006) in the context of image processing and was called *higher order total variation regularization*. It was later rediscovered by Kim et al. (2009) and termed *trend filtering* in the nonparametric regression setting. Kim et al. (2009) specifically explored linear trend filtering ($r = 1$) which fits piecewise linear models. Tibshirani et al. (2014) extensively studied trend filtering and compared its performance with smoothing splines Green and Silverman (1993) and locally adaptive regression splines Mammen et al. (1997) in the context of nonparametric regression. Tibshirani et al. (2014) also established that trend filtering enjoys desirable and strong theoretical properties of locally adaptive regression splines while being computationally less intensive due to its banded penalty matrix. Moreover, trend filtering has an adaptive knot selection property, which makes it well suited for change point analysis.

From a computational and algorithmic standpoint, Kim et al. (2009) described Primal-Dual Interior Point (PDIP) method for deriving the estimates of the linear trend filtering problem at a fixed value of λ . This can be easily carried over to the trend filtering problem of any order. Wang et al. (2014) suggested an algorithm based on a falling factorial basis while Ramdas and Tibshirani (2016) derived an algorithm based on the Alternating Direction Method of Multipliers (ADMM) discussed in Boyd et al. (2011). The computational complexity of all these algorithms is of order $O(n)$.

In this paper, we develop a new methodology called *Pattern Recovery Using Trend Filtering* (PRUTF) for identifying unknown change points in piecewise polynomial signals with no continuity restriction at change point locations. Therefore, a change point is defined as a sudden jump in the signal and its all derivatives up to order r . Figure 2 displays such change points for various r . In this paper, we make the following contributions.

- We propose a generic dual solution path algorithm along with the regularization parameter for trend filtering. This solution path, whose basic idea is borrowed from Tibshirani (2011)

enables us to determine change points at each level of the regularization parameter. Our algorithm, PRUTF, is different from that of Tibshirani (2011) as we remove $(r + 1)$ coordinates of dual variables after identifying each change point. This adjustment to the algorithm allows us to have independent dual variables between each pair of neighbouring change points. Besides, the elimination of $(r + 1)$ coordinates at each step leads to faster implementation of the algorithm.

- We establish a stopping criterion that plays an essential rule in the PRUTF algorithm used to find change points. Notably, we show that the dual variables of trend filtering between consecutive change points constitute a Gaussian bridge process. This finding allows us to introduce a threshold for terminating our proposed algorithm.
- If the signal contains a staircase pattern, we prove that the method is statistically inconsistent, which makes it unfavourable. Explaining the reason for this end, we modify the PRUTF algorithm to produce estimates consistent in terms of both the number and location of change points.

This paper is organized as follows: we first describe how to characterize the dual optimization problem of trend filtering. In Section 3, we develop our main algorithm, PRUTF, to use in constructing the dual solution path of trend filtering and, in turn, identifying the locations of change points. Section 4 discusses the properties of this dual solution path. We establish that the dual variables derived from the solution path form a Gaussian bridge process that makes them favourable for statistical inference. Applying these properties, we develop a stopping rule for the change point search algorithm in Section 5. The quality of the PRUTF algorithm is validated in terms of pattern recovery of the true signal in Section 6. It is established that the proposed technique in its naive form fails to consistently identify the true signal when a special pattern, called staircase, is present in the signal. Section 7 elaborates on how to modify the algorithm in order to estimate the true pattern consistently. Simulation results, and real-world applications are presented in Section 8. We explore the performance of our proposed method for signals with frequent change points as well as models with dependent error terms in Section 9. We conclude the paper with a discussion in Section 10.

2 Notations and Fundamental Concepts

2.1 Notations

We begin this section with setting up notations that will be used throughout this article. For an $m \times n$ matrix \mathbf{A} , we denote its rows by $\mathbf{A}_1, \dots, \mathbf{A}_m$ and express the matrix as $\mathbf{A} = (\mathbf{A}_1^T, \dots, \mathbf{A}_m^T)^T$. Now for the set of indices $\mathcal{I} = \{i_1, \dots, i_k\} \subseteq \{1, \dots, m\}$, the notation $\mathbf{A}_{\mathcal{I}} = (\mathbf{A}_{i_1}^T, \dots, \mathbf{A}_{i_k}^T)^T$ represents the submatrix of \mathbf{A} whose row labels are in the set \mathcal{I} . In a similar manner, for a vector \mathbf{a} of length m , we let $\mathbf{a}_{\mathcal{I}} = (a_{i_1}, \dots, a_{i_k})^T$ denote a subvector of \mathbf{a} whose coordinate labels are in \mathcal{I} . We write $\mathbf{A}_{-\mathcal{I}}$ and $\mathbf{a}_{-\mathcal{I}}$ to denote $\mathbf{A}_{\{1, \dots, m\} \setminus \mathcal{I}}$ and $\mathbf{a}_{\{1, \dots, m\} \setminus \mathcal{I}}$, respectively, where $\mathcal{J} \setminus \mathcal{I}$ is the set of indices in \mathcal{J} but not in \mathcal{I} . Furthermore, for selecting

i -th row of \mathbf{A} , the notation $[\mathbf{A}]_i$ and for its (i, j) -th element the notation $[\mathbf{A}]_{ij}$ are used. Also, $[\mathbf{a}]_i$ extracts the i -th elements of the vector \mathbf{a} . We write $\text{diag}(\mathbf{A})$ to denote the vector of the main diagonal entries of the matrix \mathbf{A} . Moreover, for a real number x , $\lfloor x \rfloor$ denotes the greatest integer less than or equal x , and $\lceil x \rceil$ denotes the least integer greater or equal x . For a set A , the indicator function is denoted by $\mathbb{1}(A)$.

2.2 The Dual Problem of Trend Filtering

Recall the trend filtering problem

$$\min_{\mathbf{f} \in \mathbb{R}^n} \frac{1}{2} \|\mathbf{y} - \mathbf{f}\|_2^2 + \lambda \|\mathbf{D}^{(r+1)} \mathbf{f}\|_1, \quad (3)$$

where $\lambda \geq 0$ is the regularization parameter for controlling the effect of smoothing, and the $(n - r - 1) \times n$ penalty matrix $\mathbf{D}^{(r+1)}$ is the difference operator of order $(r + 1)$. For $r = 0$, the first order difference matrix $\mathbf{D}^{(1)}$ is defined as

$$\mathbf{D}^{(1)} = \begin{pmatrix} -1 & 1 & 0 & \dots & 0 & 0 \\ 0 & -1 & 1 & \dots & 0 & 0 \\ \vdots & & & & & \vdots \\ 0 & 0 & 0 & \dots & -1 & 1 \end{pmatrix},$$

and for $r \geq 1$, the difference operator of order $r + 1$ can be recursively computed by $\mathbf{D}^{(r+1)} = \mathbf{D}^{(1)} \times \mathbf{D}^{(r)}$. Notice that, in this matrix multiplication, we consider only the submatrix consisting of the first $n - r - 2$ rows and $n - r - 1$ columns of the matrix $\mathbf{D}^{(1)}$. Figure 1 displays the trend filtering fits for $r = 0, 1, 2$ for simulated data.

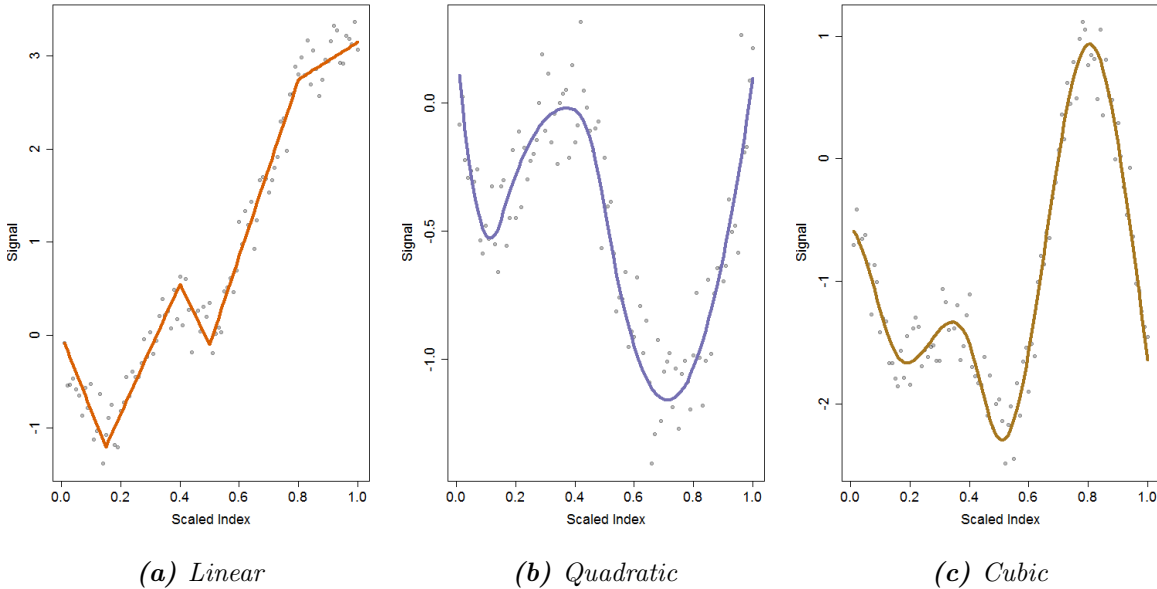


Figure 1: Trend filtering solutions for $r = 1, 2, 3$ producing (a) piecewise linear, (b) piecewise quadratic and (c) piecewise cubic fits, respectively.

Although the objective function in the r -th order trend filtering (3) is strictly convex and thus the minimization has a guaranteed unique solution, the penalty term is not differentiable

in \mathbf{f} , so solving the optimization in its current form is difficult. To overcome this difficulty, we follow the argument in [Tibshirani \(2011\)](#) and convert this optimization problem into its dual form. Since the objective function in the primal problem is strictly convex with no constraint, the strong duality holds, meaning that the primal and the dual solutions coincide.

The trend filtering problem (3) can be rewritten as

$$\min_{\mathbf{f} \in \mathbb{R}^n} \frac{1}{2} \|\mathbf{y} - \mathbf{f}\|_2^2 + \lambda \|\mathbf{z}\|_1, \quad \text{subject to } \mathbf{z} = \mathbf{D}\mathbf{f},$$

where, for ease in the notation, we use $\mathbf{D} = \mathbf{D}^{(r+1)}$. For any given $\lambda > 0$, the Lagrangian is

$$\mathcal{L}(\mathbf{f}, \mathbf{z}, \mathbf{u}) = \frac{1}{2} \|\mathbf{y} - \mathbf{f}\|_2^2 + \lambda \|\mathbf{z}\|_1 + \mathbf{u}^T (\mathbf{D}\mathbf{f} - \mathbf{z})$$

and, thus the dual function is given by

$$g(\mathbf{u}) = \inf_{\mathbf{f} \in \mathbb{R}^n, \mathbf{z} \in \mathbb{R}^m} \mathcal{L}(\mathbf{f}, \mathbf{z}, \mathbf{u}),$$

which is a concave function defined on \mathbb{R}^m , where $m = n - r - 1$ and takes values in the extended real line $\mathbb{R} \cup \{-\infty, \infty\}$. The vectors \mathbf{f} and \mathbf{u} are called the primal and dual variables, respectively. Taking the derivative of the Lagrangian $\mathcal{L}(\mathbf{f}, \mathbf{z}, \mathbf{u})$ with respect to \mathbf{f} and setting it to be equal to zero, we obtain

$$\mathbf{f} = \mathbf{y} - \mathbf{D}^T \mathbf{u}. \quad (4)$$

Now substituting this back into the Lagrangian $\mathcal{L}(\mathbf{f}, \mathbf{z}, \mathbf{u})$, and performing certain algebraic manipulations, we obtain

$$\begin{aligned} \mathcal{L}^*(\mathbf{z}, \mathbf{u}) &= \inf_{\mathbf{f} \in \mathbb{R}^n} \mathcal{L}(\mathbf{f}, \mathbf{z}, \mathbf{u}) \\ &= -\frac{1}{2} \|\mathbf{y} - \mathbf{D}^T \mathbf{u}\|_2^2 + \frac{1}{2} \|\mathbf{y}\|_2^2 + \lambda \|\mathbf{z}\|_1 - \mathbf{u}^T \mathbf{z}. \end{aligned}$$

Minimizing $\mathcal{L}^*(\mathbf{z}, \mathbf{u})$, or equivalently maximizing $\mathbf{u}^T \mathbf{z} - \lambda \|\mathbf{z}\|_1$, with respect to $\mathbf{z} \in \mathbb{R}^m$ leads us to the dual function $g(\mathbf{u})$. Notice that $\sup_{\mathbf{z}} \{\mathbf{u}^T \mathbf{z} - \lambda \|\mathbf{z}\|_1\}$ is the conjugate of the function $\lambda \|\mathbf{z}\|_1$ in the context of conjugate convex functions. See [Brezis \(2010\)](#) and [Boyd and Vandenberghe \(2004\)](#). This conjugate function is given by

$$\sup_{\mathbf{z}} \{\mathbf{u}^T \mathbf{z} - \lambda \|\mathbf{z}\|_1\} = \begin{cases} 0 & \text{if } \|\mathbf{u}\|_\infty \leq \lambda \\ \infty & \text{otherwise.} \end{cases}$$

From all these, the dual function is given as

$$g(\mathbf{u}) = -\frac{1}{2} \|\mathbf{y} - \mathbf{D}^T \mathbf{u}\|_2^2 + \frac{1}{2} \|\mathbf{y}\|_2^2 \quad \text{for } \|\mathbf{u}\|_\infty \leq \lambda,$$

and, thus the dual problem is to find the maximum of the dual function $g(\mathbf{u})$. This is equivalent to

$$\min_{\mathbf{u} \in \mathbb{R}^m} \frac{1}{2} \|\mathbf{y} - \mathbf{D}^T \mathbf{u}\|_2^2 \quad \text{subject to } \|\mathbf{u}\|_\infty \leq \lambda. \quad (5)$$

The constraint in (5) is an ℓ_∞ -ball or a hypercube centered at the origin with the boundaries given by the set $\{-\lambda, +\lambda\}^m$. Since the matrix \mathbf{D} is full row rank, the problem (5) is strictly

convex and has a unique solution, see [Ali et al. \(2019\)](#). In addition, notice that the dimension of the dual vector \mathbf{u} is m , which is smaller than that of the primal vector \mathbf{f} and may lead to relatively faster computations. The connection between the primal and the dual solutions is given by the equations

$$\hat{\mathbf{u}}_\lambda = \lambda \hat{\boldsymbol{\gamma}}, \quad (6)$$

$$\hat{\mathbf{f}}_\lambda = \mathbf{y} - \mathbf{D}^T \hat{\mathbf{u}}_\lambda, \quad (7)$$

where $\hat{\boldsymbol{\gamma}} \in \mathbb{R}^m$ is a subgradient of $\|\mathbf{x}\|_1$ computed at $\mathbf{x} = \mathbf{D}\hat{\mathbf{f}}_\lambda$. This subgradient is given by

$$\hat{\gamma}_i \in \begin{cases} \{+1\} & \text{if } [\mathbf{D}\hat{\mathbf{f}}_\lambda]_i > 0 \\ \{-1\} & \text{if } [\mathbf{D}\hat{\mathbf{f}}_\lambda]_i < 0 \\ [-1, +1] & \text{if } [\mathbf{D}\hat{\mathbf{f}}_\lambda]_i = 0. \end{cases} \quad (8)$$

The statements in Equations (6)-(8) are equivalent to the KKT optimality conditions of the primal problem (3). The dual problem (5) demonstrates that $\mathbf{D}^T \hat{\mathbf{u}}_\lambda$ is the projection, $P_{\mathbb{C}}(\mathbf{y})$, of \mathbf{y} onto the convex polyhedron (or hypercube here) $\mathbb{C} = \{\mathbf{x} \in \mathbb{R}^m : \|\mathbf{x}\|_\infty \leq \lambda\}$. From this, the primal solution (7) can be rewritten in the form of $(\mathbf{I} - P_{\mathbb{C}})(\mathbf{y})$, representing the residual projection map of \mathbf{y} onto the polyhedron \mathbb{C} .

Our idea of applying trend filtering to discover change points in piecewise polynomial signals is inspired by [Rinaldo et al. \(2009\)](#) and its correction [Rinaldo \(2014\)](#), in which change point detection is studied using fused lasso. Besides extending to piecewise polynomial signals, the novelty of our work is in providing an exact stopping criterion, which is based on the Gaussian bridge property of the trend filtering dual variables. In addition, we propose an algorithm which, unlike that proposed in [Rinaldo et al. \(2009\)](#), always produces consistent change points even in the presence of staircase patterns.

3 Solution Path of Trend Filtering and PRUTF Algorithm

In this section, we construct and study the solution path of dual variables $\hat{\mathbf{u}}_\lambda$ as the regularization parameter decreases from $\lambda = \infty$ to $\lambda = 0$. In the following, the PRUTF algorithm is given to compute the entire dual solution path. This dual solution path identifies the corresponding primal solution using (7). For any given λ , we call any coordinate of $\hat{\mathbf{u}}_\lambda$ a boundary coordinate if it is a vertex of the polyhedron $\mathbb{C} = \{\mathbf{x} \in \mathbb{R}^m : \|\mathbf{x}\|_\infty \leq \lambda\}$, meaning that its absolute value becomes λ . In the process of constructing the solution path, for any λ , we trace several sets, introduced below.

- The set $\mathcal{B} = \mathcal{B}(\lambda)$, called the boundary set, contains the boundary coordinates identified by $\hat{\mathbf{u}}_\lambda$.
- The vector $\mathbf{s}_{\mathcal{B}} = \mathbf{s}_{\mathcal{B}}(\lambda)$, called the sign vector, represents collectively the signs of the boundary points in $\mathcal{B}(\lambda)$.
- The set $\mathcal{A} = \mathcal{A}(\lambda)$, called the augmented boundary set, contains the boundary coordinates in $\mathcal{B}(\lambda)$ as well as the first $r_a = \lfloor (r + 1)/2 \rfloor$ coordinates immediately after.

- The vector $\mathbf{s}_{\mathcal{A}} = \mathbf{s}_{\mathcal{A}}(\lambda)$ represents collectively the signs of the augmented boundary points in $\mathcal{A}(\lambda)$.

In the following, we discuss the need for the augmented boundary set \mathcal{A} . We begin by studying the structure of the dual vector $\mathbf{u} = \mathbf{D}\mathbf{f}$ in a piecewise polynomial signal of order r , where the signal is partitioned into a number of blocks defined by the position of the change points. Because the signal f is a piecewise polynomial of order r , to compute the i -th coordinate of the vector \mathbf{u} , we need $r_b = \lceil (r+1)/2 \rceil - 1$ points directly before the i -th element of \mathbf{f} as well as $r_a = \lfloor (r+1)/2 \rfloor$ points immediately after that. Consequently, the first r_a elements of $\mathbf{D}\mathbf{f}$ within each block cannot be computed. Moreover, within each block, the last $r_b + 1$ elements of $\mathbf{D}\mathbf{f}$ are all nonzero due to the existence of a change point. This observation is depicted in Figure 2 for $r = 0, 1, 2, 3$. To explain this point clearly, consider the case of $r = 2$ in Figure 2 in which the structure of $\mathbf{D}\mathbf{f}$ is shown, where the true change points are at 6 and 13. As can be seen, the points on the boundary – the nonzero coordinates of $\mathbf{D}\mathbf{f}$ – are $\mathcal{B}(\lambda) = \{5, 6, 12, 13\}$ with their respective signs $\mathbf{s}_{\mathcal{B}}(\lambda) = \{1, 1, -1, -1\}$. Notice that $\mathbf{D}\mathbf{f}$ does not exist at points 7 and 14. The augmented boundary set contains these points as well as the boundary points; that is $\mathcal{A}(\lambda) = \{5, 6, 7, 12, 13, 14\}$. The respective signs of the coordinates in the augmented boundary set $\mathcal{A}(\lambda)$ are given by $\mathbf{s}_{\mathcal{A}}(\lambda) = \{1, 1, 1, -1, -1, -1\}$. At each value of λ , we call the coordinates that belong to the augmented boundary set $\mathcal{A}(\lambda)$ the augmented boundary coordinates, and the rest, the interior coordinates.

At the j -th iteration with $\lambda = \lambda_j$, we assume that the boundary set and its corresponding sign vector are $\mathcal{B} = \mathcal{B}(\lambda)$ and $\mathbf{s}_{\mathcal{B}} = \mathbf{s}_{\mathcal{B}}(\lambda)$, respectively. Furthermore, we assume the augmented boundary set and its sign vector are $\mathcal{A} = \mathcal{A}(\lambda)$ and $\mathbf{s}_{\mathcal{A}} = \mathbf{s}_{\mathcal{A}}(\lambda)$, respectively. Dual coordinates can be split into augmented boundary coordinates $\hat{\mathbf{u}}_{\lambda_j, \mathcal{A}}$ and interior coordinates $\hat{\mathbf{u}}_{\lambda_j, -\mathcal{A}}$. Recall from Section 2.1 that $\hat{\mathbf{u}}_{\lambda_j, \mathcal{A}}$ represents the subvector of $\hat{\mathbf{u}}_{\lambda}$ with the coordinate labels in the set \mathcal{A} and $\hat{\mathbf{u}}_{\lambda_j, -\mathcal{A}}$ represents the subvector of $\hat{\mathbf{u}}_{\lambda}$ with the coordinate labels in the set $\{1, 2, \dots, m\} \setminus \mathcal{A}$. It is apparent from the definition of the boundary coordinates that

$$\hat{\mathbf{u}}_{\lambda_j, \mathcal{A}} = \lambda_j \mathbf{s}_{\mathcal{A}}. \quad (9)$$

Replacing the boundary coordinate with $\lambda_j \mathbf{s}_{\mathcal{A}}$ in (5) and solving the resulting quadratic problem with respect to the interior coordinates, lead to their least square estimates, given by

$$\hat{\mathbf{u}}_{\lambda_j, -\mathcal{A}} = \left(\mathbf{D}_{-\mathcal{A}} \mathbf{D}_{-\mathcal{A}}^T \right)^{-1} \mathbf{D}_{-\mathcal{A}} (\mathbf{y} - \lambda_j \mathbf{D}_{\mathcal{A}}^T \mathbf{s}_{\mathcal{A}}). \quad (10)$$

It should be noted that for the purpose of simplicity, we denote $(\mathbf{D}_{\mathcal{A}})^T$ and $(\mathbf{D}_{-\mathcal{A}})^T$ with $\mathbf{D}_{\mathcal{A}}^T$ and $\mathbf{D}_{-\mathcal{A}}^T$, respectively. Notice that in (10), the first term $(\mathbf{D}_{-\mathcal{A}} \mathbf{D}_{-\mathcal{A}}^T)^{-1} \mathbf{D}_{-\mathcal{A}} \mathbf{y}$ simply yields the least square estimate of regressing the response vector \mathbf{y} on the design matrix $\mathbf{D}_{-\mathcal{A}}$. The second term $-\lambda_j (\mathbf{D}_{-\mathcal{A}} \mathbf{D}_{-\mathcal{A}}^T)^{-1} \mathbf{D}_{-\mathcal{A}} \mathbf{D}_{\mathcal{A}}^T \mathbf{s}_{\mathcal{A}}$ can be interpreted as a shrinkage term due to the condition $\|\mathbf{u}\|_{\infty} \leq \lambda$. The expression (10) is true for $\lambda \leq \lambda_j$ until either an interior coordinate joins to the boundary or a coordinate in the boundary set leaves the boundary. The following argument explains how to specify values of λ while the interior coordinates change.

We define the joining time associated with the interior coordinate $i \in \{1, 2, \dots, m\} \setminus \mathcal{A}$ as the time at which this interior coordinate joins the boundary. To determine the next join-

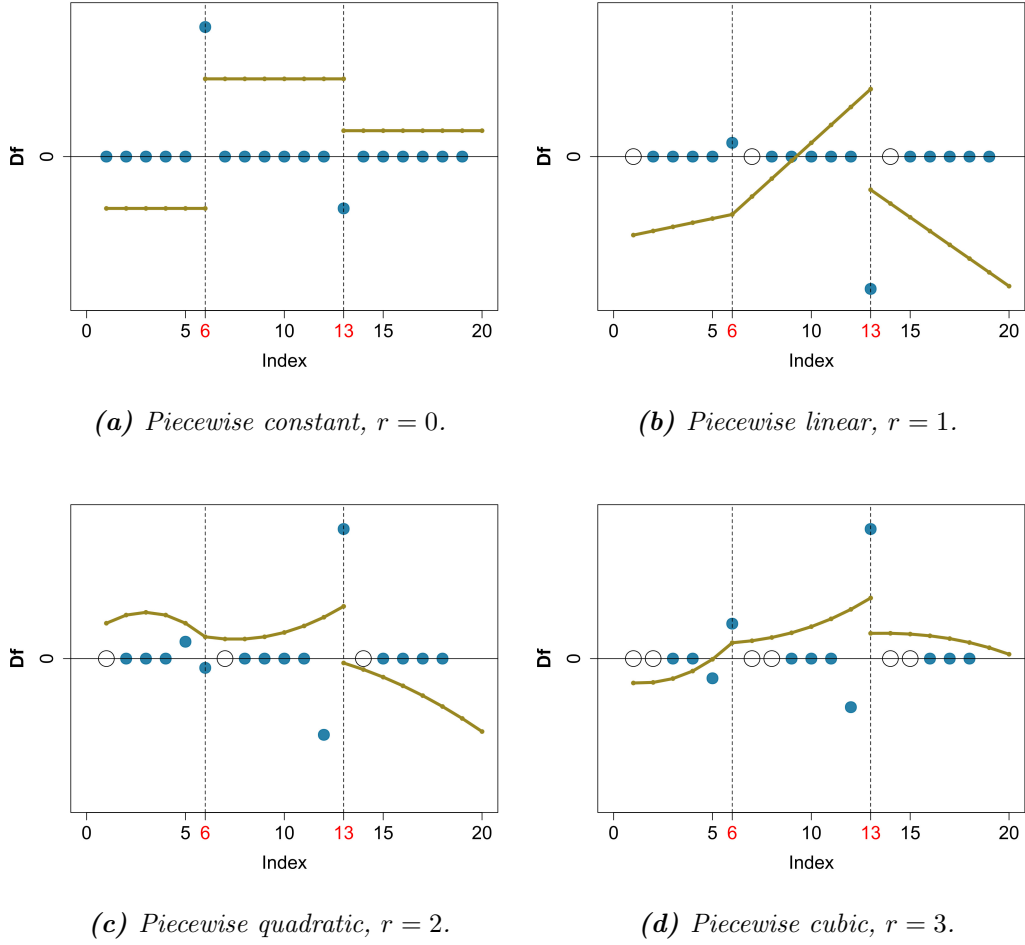


Figure 2: Structure of \mathbf{Df} for piecewise polynomial signals with various orders $r = 0, 1, 2, 3$. The olive lines display the true signals with two change points at the locations 6 and 13. Empty circles represent the indices that \mathbf{Df} does not exist.

ing time, we reduce the value of λ in a linear direction starting from λ_j and solve $\hat{\mathbf{u}}_{\lambda, -\mathcal{A}} = (\pm\lambda, \dots, \pm\lambda)^T$. Note that the right-hand side of (10) can be expressed as $\mathbf{a} - \lambda \mathbf{b}$, where

$$\begin{aligned} \mathbf{a} &= (\mathbf{D}_{-\mathcal{A}} \mathbf{D}_{-\mathcal{A}}^T)^{-1} \mathbf{D}_{-\mathcal{A}} \mathbf{y}, \\ \mathbf{b} &= (\mathbf{D}_{-\mathcal{A}} \mathbf{D}_{-\mathcal{A}}^T)^{-1} \mathbf{D}_{-\mathcal{A}} \mathbf{D}_{\mathcal{A}}^T \mathbf{s}_{\mathcal{A}}. \end{aligned} \quad (11)$$

The joining time for every $i \in \{1, 2, \dots, m\} \setminus \mathcal{A}$ is hence the solution of the equation $a_i - \lambda b_i = \pm\lambda$ with respect to λ , which is given by

$$\lambda_i^{\text{join}} = \frac{a_i}{b_i \pm 1}, \quad i \in \{1, 2, \dots, m\} \setminus \mathcal{A}.$$

Note that λ_i^{join} is uniquely defined because only one of the signs -1 or $+1$ yields $\lambda_i \in [0, \lambda_j]$.

Now we turn the attention to the characterization of a coordinate which leaves the boundary set \mathcal{B} . For $i \in \mathcal{B}$, the leaving time is defined as the time that the coordinate i leaves the boundary set \mathcal{B} . Since $\mathbf{s}_{\mathcal{B}}$ is the sign vector of changes captured by $[\mathbf{D}\hat{\mathbf{f}}]_{\mathcal{B}}$, then $\text{diag}(\mathbf{s}_{\mathcal{B}}) [\mathbf{D}\hat{\mathbf{f}}]_{\mathcal{B}} > \mathbf{0}$,

which in turn, along with Equation (7), implies $\text{diag}(\mathbf{s}_{\mathcal{B}})[\mathbf{D}(\mathbf{y} - \mathbf{D}^T \hat{\mathbf{u}}_\lambda)]_{\mathcal{B}} > \mathbf{0}$. Here, for any vector $\boldsymbol{\eta}$, $\text{diag}(\boldsymbol{\eta})$ denotes the diagonal matrix with the diagonal elements given by $\boldsymbol{\eta}$, and $\boldsymbol{\eta} > \mathbf{0}$ holds element-wise. Therefore, a coordinate $i \in \mathcal{B}$ leaves the boundary set \mathcal{B} if $\text{diag}(\mathbf{s}_{\mathcal{B}})[\mathbf{D}(\mathbf{y} - \mathbf{D}^T \hat{\mathbf{u}}_\lambda)]_{\mathcal{B}} > \mathbf{0}$ is violated. Using the relation

$$\left[\mathbf{D}(\mathbf{y} - \mathbf{D}^T \hat{\mathbf{u}}_\lambda)\right]_{\mathcal{B}} = \mathbf{D}_{\mathcal{B}}(\mathbf{y} - \mathbf{D}^T \hat{\mathbf{u}}_\lambda),$$

and the decomposition $\mathbf{D}^T \hat{\mathbf{u}}_\lambda = \mathbf{D}_{\mathcal{A}}^T \hat{\mathbf{u}}_{\lambda, \mathcal{A}} + \mathbf{D}_{-\mathcal{A}}^T \hat{\mathbf{u}}_{\lambda, -\mathcal{A}}$, we obtain

$$\text{diag}(\mathbf{s}_{\mathcal{B}})\left[\mathbf{D}(\mathbf{y} - \mathbf{D}^T \hat{\mathbf{u}}_\lambda)\right]_{\mathcal{B}} = \mathbf{c} - \lambda \mathbf{d}, \quad (12)$$

where

$$\begin{aligned} \mathbf{c} &= \text{diag}(\mathbf{s}_{\mathcal{B}}) \mathbf{D}_{\mathcal{B}}(\mathbf{y} - \mathbf{D}_{-\mathcal{A}}^T \mathbf{a}), \\ \mathbf{d} &= \text{diag}(\mathbf{s}_{\mathcal{B}}) \mathbf{D}_{\mathcal{B}}(\mathbf{D}_{\mathcal{A}}^T \mathbf{s}_{\mathcal{A}} - \mathbf{D}_{-\mathcal{A}}^T \mathbf{b}). \end{aligned} \quad (13)$$

Hence, a leaving time is obtained from the equation $c_i - \lambda d_i > 0$ as

$$\lambda_i^{\text{leave}} = \begin{cases} \frac{c_i}{d_i}, & \text{if } c_i < 0 \text{ and } d_i < 0, \\ 0, & \text{otherwise.} \end{cases}$$

The conditions in the aforementioned equation is due to the fact that at the j -th iteration with $\lambda \leq \lambda_j$, the expression $c_i - \lambda d_i > 0$ fails for $i \in \mathcal{B}$, if both c_i and d_i are negative. An alternative way to determine the next leaving time is to use the KKT optimality conditions of (5). We refer the reader to the supplementary materials of Tibshirani (2011).

The following algorithm, PRUTF, describes the process of constructing the entire dual solution path of trend filtering.

Algorithm 1 (PRUTF Algorithm)

1. Initialize the set of change points locations as $\boldsymbol{\tau}_0 = \emptyset$, the empty set.
2. At step $j = 1$, initialize the boundary set $\mathcal{B}_1 = \{\tau_1 - r_b, \tau_1 - r_b + 1, \dots, \tau_1\}$ and its associated sign vector $\mathbf{s}_{\mathcal{B}_1} = \{s_1, \dots, s_1\}$, both with cardinality of $r_b + 1$, where τ_1 is obtained by

$$\tau_1 = \underset{i=1, \dots, m}{\text{argmax}} |\hat{u}_i|, \quad (14)$$

and $s_1 = \text{sign}(\hat{u}_{\tau_1})$, where \hat{u}_i is the i -th element of the vector $\hat{\mathbf{u}} = (\mathbf{D}\mathbf{D}^T)^{-1} \mathbf{D}\mathbf{y}$. The updated set of change points locations is now $\boldsymbol{\tau}_1 = \{\tau_1\}$. We also record the first joining time $\lambda_1 = |\hat{u}_{\tau_1}|$ and keep track of the augmented boundary set $\mathcal{A}_1 = \{\tau_1 - r_b, \dots, \tau_1 + r_a\}$ and its corresponding sign vector $\mathbf{s}_{\mathcal{A}_1} = \{s_1, \dots, s_1\}$ of length $r + 1$. The dual solution is regarded as $\hat{\mathbf{u}}(\lambda) = (\mathbf{D}\mathbf{D}^T)^{-1} \mathbf{D}\mathbf{y}$, for $\lambda \geq \lambda_1$.

3. For step $j = 2, 3, \dots$,

(a) Obtain the pair $(\tau_j^{\text{join}}, s_j^{\text{join}})$ from

$$(\tau_j^{\text{join}}, s_j^{\text{join}}) = \underset{i \notin \mathcal{A}_{j-1}, s \in \{-1, 1\}}{\operatorname{argmax}} \frac{a_i}{s + b_i} \cdot \mathbb{1} \left\{ 0 \leq \frac{a_i}{s + b_i} \leq \lambda_{j-1} \right\}, \quad (15)$$

and set the next joining time λ_j^{join} as the value of $\frac{a_i}{s + b_i}$, for $i = \tau_j^{\text{join}}$ and $s = s_j^{\text{join}}$.

(b) Obtain the pair $(\tau_j^{\text{leave}}, s_j^{\text{leave}})$ from

$$(\tau_j^{\text{leave}}, s_j^{\text{leave}}) = \underset{i \in \mathcal{B}_{j-1}, s \in \{-1, 1\}}{\operatorname{argmax}} \frac{c_i}{d_i} \cdot \mathbb{1} \left\{ c_i < 0, d_i < 0 \right\}, \quad (16)$$

and assign the next leaving time λ_j^{leave} as the value of $\frac{c_i}{d_i}$, for $i = \tau_j^{\text{leave}}$ and $s = s_j^{\text{leave}}$.

(c) Let $\lambda_j = \max \{ \lambda_j^{\text{join}}, \lambda_j^{\text{leave}} \}$, then the boundary set \mathcal{B}_j and its sign vector $\mathbf{s}_{\mathcal{B}_j}$ are updated in the following fashion:

- Either append $\{ \tau_j^{\text{join}} - r_b, \tau_j^{\text{join}} - r_b + 1, \dots, \tau_j^{\text{join}} \}$ and the corresponding signs $\{ s_j^{\text{join}}, \dots, s_j^{\text{join}} \}$ to \mathcal{B}_{j-1} and $\mathbf{s}_{\mathcal{B}_{j-1}}$, respectively, provided that $\lambda_j = \lambda_j^{\text{join}}$. Also, add τ_j^{join} to $\boldsymbol{\tau}_{j-1}$.
- Or remove $\{ \tau_j^{\text{leave}}, \tau_j^{\text{leave}} + 1, \dots, \tau_j^{\text{leave}} + r_b \}$ and the corresponding signs $\{ s_j^{\text{leave}}, \dots, s_j^{\text{leave}} \}$ from \mathcal{B}_{j-1} and $\mathbf{s}_{\mathcal{B}_{j-1}}$, respectively, provided that $\lambda_j = \lambda_j^{\text{leave}}$. Also, remove τ_j^{leave} from $\boldsymbol{\tau}_{j-1}$.

In the same manner, the augmented boundary set, \mathcal{A}_j and its sign, $\mathbf{s}_{\mathcal{A}_j}$ are formed by adding $\{ \tau_j^{\text{join}} - r_b, \dots, \tau_j^{\text{join}} + r_a \}$ and $\{ s_j^{\text{join}}, \dots, s_j^{\text{join}} \}$ to \mathcal{A}_{j-1} and $\mathbf{s}_{\mathcal{A}_{j-1}}$, respectively, if $\lambda_j = \lambda_j^{\text{leave}}$ or, otherwise, by removing the associated set $\{ \tau_j^{\text{leave}}, \dots, \tau_j^{\text{leave}} + r \}$ and $\{ s_j^{\text{leave}}, \dots, s_j^{\text{leave}} \}$ from \mathcal{A}_{j-1} and $\mathbf{s}_{\mathcal{A}_{j-1}}$. Thus, the dual solution is computed as $\hat{\mathbf{u}}_{\mathcal{A}_j}(\lambda) = \mathbf{a} - \lambda \mathbf{b}$ for interior coordinates and $\hat{\mathbf{u}}_{-\mathcal{A}_j}(\lambda) = \lambda \mathbf{s}_{\mathcal{A}_j}$ for boundary coordinates over $\lambda_j \leq \lambda \leq \lambda_{j-1}$.

4. Repeat step 3 until $\lambda_j > 0$.

The critical points $\lambda_1 \geq \lambda_2 \geq \dots \geq 0$ indicate the values of the regularization parameter at which the boundary set changes.

Remark 1 Notice that the vector $\boldsymbol{\tau}$ derived by the PRUTF algorithm represents the locations of change points for the dual variables. In order to obtain the locations of change points in primal variables, we must add r_a to any element of $\boldsymbol{\tau}$, that is, $\{ \tau_1 + r_a, \tau_2 + r_a, \dots \}$. This relationship between the primal and dual change point sets is visible from Figure 2.

Remark 2 For fused lasso, $r = 0$, Lemma 1 of Tibshirani (2011), known as the boundary lemma, is satisfied since the matrix $\mathbf{D}\mathbf{D}^T$ is diagonally dominant, meaning that $[\mathbf{D}\mathbf{D}^T]_{i,i} \geq \sum_{j \neq i} |[\mathbf{D}\mathbf{D}^T]_{i,j}|$, for $i = 1, \dots, m$. This lemma states that when a coordinate joins the boundary, it will stay on the boundary for the rest of the path. Consequently, part (b) of step 3 in Algorithm 1 is unnecessary, and hence the next leaving time in part (c) is set to zero, i.e., $\lambda_j^{\text{leave}} = 0$, for every step j . However, the boundary lemma is not satisfied for $r = 1, 2, 3, \dots$

Remark 3 *There is a subtle and important distinction between our proposed algorithm, PRUTF, and the one presented in Tibshirani (2011). The latter work studies the generalized lasso problem for any arbitrary penalty matrix \mathbf{D} (unlike \mathbf{D} used in trend filtering, which must have a certain structure). The proposed algorithm in Tibshirani (2011) relies on adding or removing only one coordinate to or from the boundary set at every step. The key attribute of our algorithm is to add or remove $r + 1$ coordinates to or from the augmented boundary set, an approach inspired by the argument presented at the beginning of this section. Essentially, this attribute makes PRUTF, presented in Algorithm 1, well-suited for change point analysis. It is important to mention that PRUTF requires at least $r + 1$ data points between neighbouring change points.*

Remark 4 *For a given λ , equations (9) and (10) give the values of the dual variables in $\hat{\mathbf{u}}_\lambda$. The equations demonstrate that the dual solution path is a linear function of λ with change in the slopes at joining or leaving times $\lambda_1 \geq \lambda_2 \geq \dots \geq 0$.*

Remark 5 *The number of iterations required for PRUTF, presented in Algorithm 1, is at most $(3^p + 1)/2$, where $p = \lceil \frac{m}{r+1} \rceil$, see Tibshirani et al. (2013), Lemma 6. However, this upper bound for the number of iterations is usually very loose. The upper bound comes from the following realization discovered by Osborne et al. (2000) and later improved by Mairal and Yu (2012). Any pair $(\mathcal{A}, \mathbf{s}_\mathcal{A})$ appears at most once throughout the solution path. In other words, if $(\mathcal{A}, \mathbf{s}_\mathcal{A})$ is visited in one iteration of the algorithm, the pair $(\mathcal{A}, -\mathbf{s}_\mathcal{A})$ as well as $(\mathcal{A}, \mathbf{s}_\mathcal{A})$ cannot reappear again for the rest of the algorithm. Interestingly, this fact says that once a coordinate enters the boundary set, it cannot immediately leave the boundary set at the next step.*

Moreover, note that at one iteration of the PRUTF algorithm with the augmented boundary set \mathcal{A} , the dominant computation is in solving the least square problem

$$\min_{\mathbf{u} \in \mathbb{R}^m} \frac{1}{2} \|\mathbf{y} - \mathbf{D}_\mathcal{A}^T \mathbf{u}\|_2^2. \quad (17)$$

One can apply QR decomposition of $\mathbf{D}_\mathcal{A}^T$ to solve the least square problem, and then update the decomposition as set \mathcal{A} changes. However, since $\mathbf{D}_{-\mathcal{A}} \mathbf{D}_{-\mathcal{A}}^T$ is a banded Toeplitz matrix (see Section 4), a solution of (17) always exists and can be computed using a banded Cholesky decomposition. Thus, the computational complexity for the iteration is of order $O((m - |\mathcal{A}|)r^2)$, which is linear in the number of interior coordinates as r is fixed and usually small. Overall, if K is the total number of steps run by the PRUTF algorithm, then the total computational complexity is $O(K(m - |\mathcal{A}|)r^2)$. See Tibshirani (2011) and Arnold and Tibshirani (2016).

4 Statistical Properties of the Solution Path

An important component of the methodology that we develop in this work involves computing algebraic expressions based on the matrix $\mathbf{D} = \mathbf{D}^{(r+1)}$. In this section, we describe the properties of such expressions. To begin with, let $\mathcal{A} = \{A_1, \dots, A_J\}$ and $\mathbf{s}_\mathcal{A} = \{\mathbf{s}_1, \dots, \mathbf{s}_J\}$ be the augmented boundary set and its corresponding sign vector, respectively, after a number of iterations of Algorithm 1, where $A_j = \{\tau_j - r_b, \tau_j - r_b + 1, \dots, \tau_j + r_a\}$ and $\mathbf{s}_j = \{s_j, \dots, s_j\}$ for $j = 1, \dots, J$. This augmented boundary set corresponds to J change points $\{\tau_1, \dots, \tau_J\}$

$$\begin{pmatrix} 6 & -4 & 1 & 0 & 0 & 0 & 0 & 0 & 0 \\ -4 & 6 & -4 & 1 & 0 & 0 & 0 & 0 & 0 \\ 1 & -4 & 6 & -4 & 1 & 0 & 0 & 0 & 0 \\ 0 & 1 & -4 & 6 & -4 & 1 & 0 & 0 & 0 \\ 0 & 0 & 1 & -4 & 6 & -4 & 1 & 0 & 0 \\ 0 & 0 & 0 & 1 & -4 & 6 & -4 & 1 & 0 \\ 0 & 0 & 0 & 0 & 1 & -4 & 6 & -4 & 1 \\ 0 & 0 & 0 & 0 & 0 & 1 & -4 & 6 & -4 \\ 0 & 0 & 0 & 0 & 0 & 0 & 1 & -4 & 6 \end{pmatrix} \quad \begin{pmatrix} 6 & -4 & 1 & | & 0 & 0 & 0 & 0 \\ -4 & 6 & -4 & | & 0 & 0 & 0 & 0 \\ 1 & -4 & 6 & | & 0 & 0 & 0 & 0 \\ \hline 0 & 0 & 0 & | & 6 & -4 & 1 & 0 \\ 0 & 0 & 0 & | & -4 & 6 & -4 & 1 \\ 0 & 0 & 0 & | & 1 & -4 & 6 & -4 \\ 0 & 0 & 0 & | & 0 & 1 & -4 & 6 \end{pmatrix}$$

(a) Structure of \mathbf{DD}^T .

(b) The structure of $\mathbf{D}_{-\mathcal{A}}\mathbf{D}_{-\mathcal{A}}^T$.

Figure 3: Structure of quadratic forms of matrix \mathbf{D} .

that partition all the dual variables into $J+1$ blocks $B_j = \{\tau_j + 1, \dots, \tau_{j+1}\}$ for $j = 0, 1, \dots, J$, with the conventions that $\tau_0 = 0$ and $\tau_{J+1} = m$. In the following, we list some properties of matrix multiplications involving \mathbf{D} .

- It follows from the definition of the matrix \mathbf{D} that it is a banded Toeplitz matrix with bandwidth $r + 1$. It turns out that the matrix \mathbf{DD}^T reveals the same property, meaning that it is a square banded Toeplitz matrix. Moreover, its $r + 1$ nonzero row elements are consecutive binomial coefficients of order $2r + 2$ with alternating signs. In other words, (i, j) -th element of \mathbf{DD}^T for $i \geq j$ is $(-1)^{i-j} \binom{2r+2}{r+1+i-j}$. An example, for $r = 1$, is given in panel (a) of Figure 3. Note that \mathbf{DD}^T is a symmetric, nonsingular and positive definite matrix (Demetriou and Lipitakis, 2001).
- The matrix $\mathbf{D}_{-\mathcal{A}}\mathbf{D}_{-\mathcal{A}}^T$ is a block diagonal matrix whose diagonal submatrices correspond to $J + 1$ blocks. More precisely, the j -th submatrix on the diagonal of $\mathbf{D}_{-\mathcal{A}}\mathbf{D}_{-\mathcal{A}}^T$ is a matrix with the first $(\tau_{j+1} - \tau_j - r)$ rows and columns of \mathbf{DD}^T , see panel (b) of Figure 3. Notice that, due to its non-singularity, $\mathbf{D}_{-\mathcal{A}}\mathbf{D}_{-\mathcal{A}}^T$ is always invertible. In fact, both $(\mathbf{D}_{-\mathcal{A}}\mathbf{D}_{-\mathcal{A}}^T)^{-1}$ and $(\mathbf{D}_{-\mathcal{A}}\mathbf{D}_{-\mathcal{A}}^T)^{-1}\mathbf{D}_{-\mathcal{A}}$ are block diagonal matrices. Another interesting result is that every row of the matrix $(\mathbf{D}_{-\mathcal{A}}\mathbf{D}_{-\mathcal{A}}^T)^{-1}\mathbf{D}_{-\mathcal{A}}$ is a contrast vector, meaning that for any $t = 1, \dots, m$,

$$\sum_{i=1}^n \left[(\mathbf{D}_{-\mathcal{A}}\mathbf{D}_{-\mathcal{A}}^T)^{-1}\mathbf{D}_{-\mathcal{A}} \right]_{t,i} = 0.$$

- Another interesting term in analyzing the behaviour of the dual variables is $\mathbf{D}_{\mathcal{A}}^T \mathbf{s}_{\mathcal{A}}$. It can be shown that the vector $\mathbf{D}_{\mathcal{A}}^T \mathbf{s}_{\mathcal{A}}$ can be partitioned into $J + 1$ subvectors associated with the change points τ_j , $j = 1, \dots, J$. The subvector associated with τ_j , $j = 2, \dots, J - 1$, is $\mathbf{D}_{\mathcal{A}_j}^T \mathbf{s}_{\mathcal{A}_j}$, whose elements are zero, except the first consecutive $r + 1$ as well as the last consecutive $r + 1$ elements. The first $r + 1$ nonzero elements of $\mathbf{D}_{\mathcal{A}_j}^T \mathbf{s}_{\mathcal{A}_j}$ are the binomial coefficients in the expansion of $s_j (x - 1)^r$, and its last $r + 1$ elements are the binomial coefficients in the expansion of $-s_{j+1} (x - 1)^r$. Furthermore, the first $r + 1$ elements of the

first subvector and the last $r + 1$ elements of the last subvector are also equal to zero. For example, for a piecewise cubic signal, $r = 3$, with two change points (τ_1, τ_2) and signs $(-1, 1)$, the vector $\mathbf{D}_{\mathcal{A}}^T \mathbf{s}_{\mathcal{A}}$ becomes

$$\left(\underbrace{0, \dots, 0, 1, -3, 3, -1}_{1:(\tau_1+r_a)}, \underbrace{-1, 3, -3, 1, 0, \dots, 0, -1, 3, -3, 1}_{(\tau_1+r_a+1):(\tau_2+r_a)}, \underbrace{1, -3, 3, -1, 0, \dots, 0}_{(\tau_2+r_a+1):m} \right).$$

Consequently, the structure of $\mathbf{D}_{A_j}^T \mathbf{s}_{A_j}$ allows us to write $\mathbf{D}_{\mathcal{A}}^T \mathbf{s}_{\mathcal{A}} = \sum_{j=0}^J \mathbf{D}_{A_j}^T \mathbf{s}_j$. Additionally, if the signs of two consecutive change points τ_j and τ_{j+1} are the same, then

$$\left[(\mathbf{D}_{-\mathcal{A}} \mathbf{D}_{-\mathcal{A}}^T)^{-1} \mathbf{D}_{-\mathcal{A}} \right]_t \left(\mathbf{D}_{A_{j+1}}^T \mathbf{s}_{j+1} + \mathbf{D}_{A_j}^T \mathbf{s}_j \right) = -s_j, \quad (18)$$

for $t = \tau_j + r_a, \dots, \tau_{j+1} + r_b$.

- Let $\mathbf{P}_D = \mathbf{D}_{-\mathcal{A}}^T (\mathbf{D}_{-\mathcal{A}} \mathbf{D}_{-\mathcal{A}}^T)^{-1} \mathbf{D}_{-\mathcal{A}}$ be the projection matrix onto the row space of the matrix $\mathbf{D}_{-\mathcal{A}}$. Moreover, let \mathbf{X}_j be the design matrix of the r -th polynomial regression on the indices of j -th segment $\{\tau_j + 1, \dots, \tau_{j+1}\}$, that is,

$$\mathbf{X}_j = \begin{pmatrix} 1 & \frac{\tau_j+1}{n} & \left(\frac{\tau_j+1}{n}\right)^2 & \dots & \left(\frac{\tau_j+1}{n}\right)^r \\ 1 & \frac{\tau_j+2}{n} & \left(\frac{\tau_j+2}{n}\right)^2 & \dots & \left(\frac{\tau_j+2}{n}\right)^r \\ \vdots & \vdots & \vdots & & \vdots \\ 1 & \frac{\tau_{j+1}}{n} & \left(\frac{\tau_{j+1}}{n}\right)^2 & \dots & \left(\frac{\tau_{j+1}}{n}\right)^r \end{pmatrix}.$$

Therefore, the orthogonal projection matrix $\mathbf{I} - \mathbf{P}_D$ is a block diagonal matrix whose j -th block associated with the segment $\{\tau_j + 1, \dots, \tau_{j+1}\}$ is equal to the projection map onto the column space of \mathbf{X}_j , i.e.,

$$\mathbf{I} - \mathbf{P}_D = \mathbf{X}_j (\mathbf{X}_j^T \mathbf{X}_j)^{-1} \mathbf{X}_j^T. \quad (19)$$

Equation (9) says that the absolute values of the boundary coordinates are λ , that is,

$$\hat{u}(t; \lambda) = \lambda s_j \quad \text{for } t \in A_j. \quad (20)$$

On the other hand, the values of the interior coordinates are given by

$$\hat{u}(t; \lambda) = \begin{cases} \left[(\mathbf{D}_{-\mathcal{A}} \mathbf{D}_{-\mathcal{A}}^T)^{-1} \mathbf{D}_{-\mathcal{A}} \right]_t \left(\mathbf{y} - \lambda \mathbf{D}_{A_1}^T \mathbf{s}_1 \right), & 1 \leq t < \tau_1 - r_b \\ \left[(\mathbf{D}_{-\mathcal{A}} \mathbf{D}_{-\mathcal{A}}^T)^{-1} \mathbf{D}_{-\mathcal{A}} \right]_t \left(\mathbf{y} - \lambda \left(\mathbf{D}_{A_{j+1}}^T \mathbf{s}_{j+1} + \mathbf{D}_{A_j}^T \mathbf{s}_j \right) \right), & \tau_j + r_a < t < \tau_{j+1} - r_b \\ \left[(\mathbf{D}_{-\mathcal{A}} \mathbf{D}_{-\mathcal{A}}^T)^{-1} \mathbf{D}_{-\mathcal{A}} \right]_t \left(\mathbf{y} - \lambda \mathbf{D}_{A_J}^T \mathbf{s}_J \right), & \tau_J + r_a < t \leq m. \end{cases} \quad (21)$$

For a given λ , the dual variables $\hat{u}(t; \lambda)$ for $t = 0, \dots, m$ can be collectively viewed as a random bridge, that is, a conditioned random walk with drift whose end points are set to zero. Moreover, $\hat{u}(t; \lambda)$ is bounded between $-\lambda$ and λ . The quantity $\hat{u}(t; \lambda)$ can also be decomposed into a sum of several smaller random bridges which are formed by blocks created from the

change points. Recall that the last consecutive $r_b + 1$ elements of the block B_j are λs_j , for any $j = 0, 1, \dots, J$. Hence, for $t = \tau_j + r_a, \dots, \tau_{j+1} - r_b$, the random bridge associated with the j -th block is given by

$$\widehat{u}_j(t; \lambda) = \left[(\mathbf{D}_{-\mathcal{A}} \mathbf{D}_{-\mathcal{A}}^T)^{-1} \mathbf{D}_{-\mathcal{A}} \right]_t \left(\mathbf{y} - \lambda (\mathbf{D}_{A_{j+1}}^T \mathbf{s}_{j+1} + \mathbf{D}_{A_j}^T \mathbf{s}_j) \right), \quad j = 0, \dots, J, \quad (22)$$

with the conventions $\mathbf{s}_0 = \mathbf{s}_{J+1} = \mathbf{0} \in \mathbb{R}^{r+1}$. It is important to note that similar to $\widehat{u}(t; \lambda)$, the process $\widehat{u}_j(t; \lambda)$ satisfies the conditions $\widehat{u}_j(\tau_j + r_a; \lambda) = \lambda s_j$ and $\widehat{u}_j(\tau_{j+1} - r_b; \lambda) = \lambda s_{j+1}$. From (22), the process $\widehat{u}_j(t; \lambda)$ is composed of the stochastic term

$$\widehat{u}_j^{\text{st}}(t) = \left[(\mathbf{D}_{-\mathcal{A}} \mathbf{D}_{-\mathcal{A}}^T)^{-1} \mathbf{D}_{-\mathcal{A}} \right]_t \mathbf{y}, \quad (23)$$

and the drift term

$$\widehat{u}_j^{\text{dr}}(t; \lambda) = -\lambda \left[(\mathbf{D}_{-\mathcal{A}} \mathbf{D}_{-\mathcal{A}}^T)^{-1} \mathbf{D}_{-\mathcal{A}} \right]_t \left(\mathbf{D}_{A_{j+1}}^T \mathbf{s}_{j+1} + \mathbf{D}_{A_j}^T \mathbf{s}_j \right). \quad (24)$$

According to model (1) with Gaussian noises, it turns out that the discrete time stochastic process term $\widehat{u}_j^{\text{st}}(t)$ can be embedded in a continuous time Gaussian bridge process. The following theorem describes the characteristics of this process.

Theorem 1 *Suppose the observation vector \mathbf{y} is drawn from the model (1), where the error vector $\boldsymbol{\varepsilon}$ has a Gaussian distribution with mean zero and covariance matrix $\sigma^2 \mathbf{I}$. For given \mathbf{D} and \mathcal{A} ,*

(a) *Define*

$$W_j(t) = (\tau_{j+1} - \tau_j - r)^{-(2r+1)/2} \left[(\mathbf{D}_{-\mathcal{A}} \mathbf{D}_{-\mathcal{A}}^T)^{-1} \mathbf{D}_{-\mathcal{A}} \right]_{\lfloor mt \rfloor} \mathbf{y}, \quad (25)$$

for $(\tau_j + r_a)/m \leq t \leq (\tau_{j+1} - r_b)/m$, where

$$W_j\left(\frac{\tau_j + r_a}{m}\right) = W_j\left(\frac{\tau_{j+1} - r_b}{m}\right) = 0, \quad (26)$$

and, for $j = 0, \dots, J$. Then the stochastic process $\mathbf{W}_j = \{W_j(t) : (\tau_j + r_a)/m \leq t \leq (\tau_{j+1} - r_b)/m\}$ is a Gaussian bridge process with mean vector zero and covariance function

$$\text{Cov}\left(W_j(t), W_j(t')\right) = \sigma^2 \left[(\mathbf{D}_{-\mathcal{A}} \mathbf{D}_{-\mathcal{A}}^T)^{-1} \right]_{\lfloor mt \rfloor, \lfloor mt' \rfloor}, \quad (27)$$

for any $(\tau_j + r_a)/m \leq t, t' \leq (\tau_{j+1} - r_b)/m$.

(b) *The processes \mathbf{W}_j and $\mathbf{W}_{j'}$ are independent, for $j' \neq j$.*

A proof is given in Appendix A.1.

This theorem could be extended to the case of non-Gaussian random variables and therefore establishes a Donsker type Central Limit Theorem for \mathbf{W}_j . Theorem 1 guarantees that the dual variable process associated with the j -th block, i.e.

$$\mathbf{u}_j = \left\{ \widehat{u}(\lfloor mt \rfloor; \lambda) : (\tau_j + r_a)/m \leq t \leq (\tau_{j+1} - r_b)/m \right\}$$

is a Gaussian bridge process with the drift term

$$-\lambda \left[(\mathbf{D}_{-\mathcal{A}} \mathbf{D}_{-\mathcal{A}}^T)^{-1} \mathbf{D}_{-\mathcal{A}} \right]_{\lfloor mt \rfloor} \left(\mathbf{D}_{A_{j+1}}^T \mathbf{s}_{j+1} + \mathbf{D}_{A_j}^T \mathbf{s}_j \right), \quad (28)$$

and the covariance matrix stated in (27).

Recall that a standard Brownian bridge process defined on the interval $[a, b]$ is a standard Brownian motion $B(t)$ conditioned on the event $B(a) = B(b) = 0$. It is often characterized from a Brownian motion $B(t)$ with $B(a) = 0$, by setting

$$B_0(t) = B(t) - \frac{t-a}{b-a} B(b).$$

The mean and covariance functions of the Brownian bridge $B_0(t)$ are given by $E(B_0(t)) = 0$ and $\text{Cov}(B_0(s), B_0(t)) = \min\{s-a, t-a\} - (b-a)^{-1}(s-a)(t-a)$ for any $s, t \in [a, b]$, respectively. A Gaussian bridge process is an extension of the Brownian bridge process when the Brownian motion $B(t)$, in the definition of the Brownian bridge $B_0(t)$, is replaced by a more general Gaussian process $G(t)$. See, for example, [Gasbarra et al. \(2007\)](#).

Remark 6 *The celebrated Donsker theorem [Donsker \(1951\)](#) states that the partial sum process of a sequence of i.i.d. random variables, with mean zero and variance 1, converges weakly to a Brownian bridge process. See [Van Der Vaart and Wellner \(1996\)](#) or [Billingsley \(2013\)](#). A version of Theorem 1 involving non-Gaussian random variables would extend this result to weighted partial sum processes and show that the limiting process is a Gaussian bridge with a certain covariance structure. So the Gaussian assumption in Theorem 1 is not restrictive. It is also interesting to show that for $r = 0, 1$, the process $\widehat{u}_j^{st}(\lfloor mt \rfloor)$ boils down to its respective CUSUM processes. To show this, consider the interval $[(\tau_j + r_a)/m, (\tau_{j+1} - r_b)/m]$,*

- For the piecewise constant signals, $r = 0$, the quantity $\left[(\mathbf{D}_{-\mathcal{A}} \mathbf{D}_{-\mathcal{A}}^T)^{-1} \mathbf{D}_{-\mathcal{A}} \right]_{\lfloor mt \rfloor} \mathbf{y}$ can be written as

$$\left(0, \dots, \underbrace{0}_{\tau_j}, 1 - \frac{\lfloor mt \rfloor}{\tau_{j+1} - \tau_j}, \dots, \underbrace{1 - \frac{\lfloor mt \rfloor}{\tau_{j+1} - \tau_j}}_{\lfloor mt \rfloor}, -\frac{\lfloor mt \rfloor}{\tau_{j+1} - \tau_j}, \dots, -\frac{\lfloor mt \rfloor}{\tau_{j+1} - \tau_j}, \underbrace{0}_{\tau_{j+1}}, \dots, 0 \right) \mathbf{y}.$$

Notice that the above statement is the CUSUM statistic for the j -th segment, that is

$$\sum_{k=\tau_j+1}^{\lfloor mt \rfloor} \left(y_k - \bar{y}_{(\tau_j+1):\tau_{j+1}} \right), \quad (29)$$

where $\bar{y}_{(\tau_j+1):\tau_{j+1}}$ is the sample average of $(y_{\tau_j+1}, \dots, y_{\tau_{j+1}})$. It is well known that the CUSUM statistic (29) converges weakly to the Brownian bridge. In addition, for any $(\tau_j + r_a)/m \leq t' \leq t \leq (\tau_{j+1} - r_b)/m$, the covariance function becomes

$$\left[(\mathbf{D}_{-\mathcal{A}} \mathbf{D}_{-\mathcal{A}}^T)^{-1} \right]_{(\lfloor mt' \rfloor, \lfloor mt \rfloor)} = (\lfloor mt' \rfloor - \tau_j) - \frac{(\lfloor mt' \rfloor - \tau_j)(\lfloor mt \rfloor - \tau_j)}{\tau_{j+1} - \tau_j},$$

which is identical to the covariance function of the Brownian bridge.

- For the piecewise linear signals $r = 1$, the quantity $\left[(\mathbf{D}_{-\mathcal{A}} \mathbf{D}_{-\mathcal{A}}^T)^{-1} \mathbf{D}_{-\mathcal{A}} \right]_{\lfloor mt \rfloor} \mathbf{y}$ reduces to

$$\sum_{k=\tau_j+1}^{\lfloor mt \rfloor} k (y_k - \hat{f}_k), \quad (30)$$

where \hat{f} is the least square fit of the simple linear regression of $(y_{\tau_j+1}, \dots, y_{\tau_{j+1}})$ onto $(\tau_j+1, \dots, \tau_{j+1})$. As proved in Theorem 1, the preceding statistic (30) is also a Gaussian bridge process. Furthermore, using the results in Hoskins and Ponzo (1972), for any $(\tau_j + r_a)/m \leq t' \leq t \leq (\tau_{j+1} - r_b)/m$, the covariance function of this Gaussian bridge process is given by

$$\begin{aligned} \left[(\mathbf{D}_{-\mathcal{A}} \mathbf{D}_{-\mathcal{A}}^T)^{-1} \right]_{(\lfloor mt' \rfloor, \lfloor mt \rfloor)} &= \frac{(\Delta_j - \lfloor mt \rfloor + \tau_j)(\Delta_j - \lfloor mt \rfloor + \tau_j + 1)}{3 \Delta_j (\Delta_j + 1) (\Delta_j + 2)} \\ &\times (\lfloor mt' \rfloor - \tau_j)(\lfloor mt' \rfloor - \tau_j + 1) \\ &\times \left[(\lfloor mt \rfloor - \tau_j + 1)(\lfloor mt' \rfloor - \tau_j - 1)(\Delta_j + 2) - (\lfloor mt \rfloor - \tau_j)(\lfloor mt' \rfloor - \tau_j + 2)\Delta_j \right], \end{aligned}$$

where $\Delta_j = \tau_{j+1} - \tau_j$.

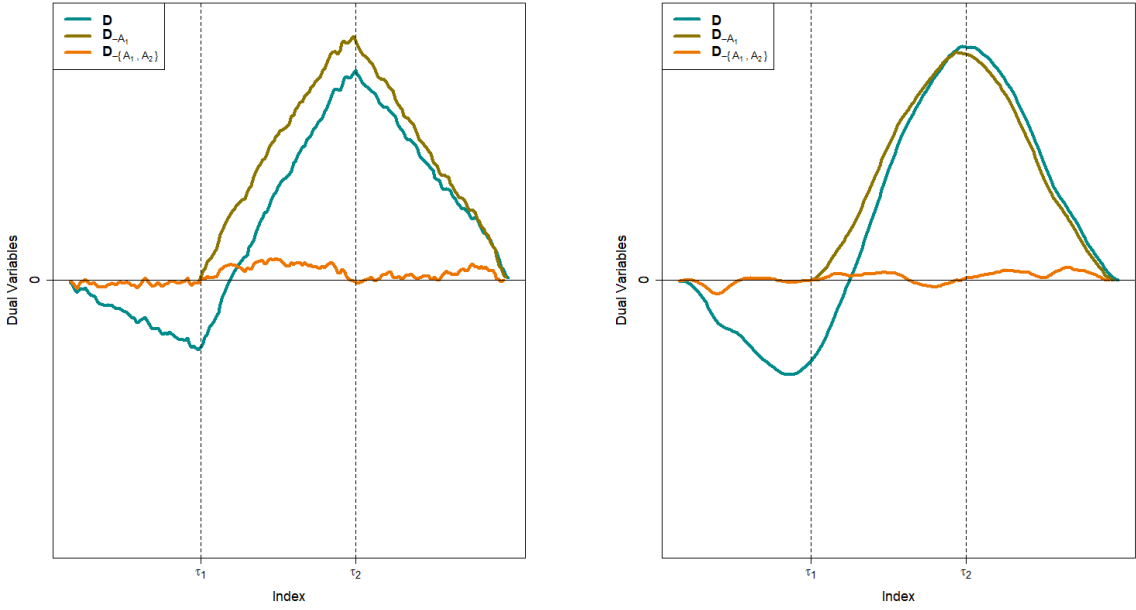
5 Stopping Criterion

This section concerns developing a stopping criterion for the PRUTF algorithm. We provide tools for deriving a threshold value at which the PRUTF algorithm terminates the search if no values of dual variables exceed this threshold. Consider the dual variables at the first step of the algorithm, i.e. $\hat{u}^{\text{st}}(t) = [(\mathbf{D}\mathbf{D}^T)^{-1} \mathbf{D}]_t \mathbf{y}$, for $t = 0, \dots, m$, which correspond to $\hat{u}^{\text{st}}(t)$ in (23) with $\mathcal{A} = \emptyset$. It turns out that $\hat{u}^{\text{st}}(t)$ is a stochastic process with local minima and maxima attained at the change points. This structure is displayed with cyan-colored lines (—) in Figure 4 for both piecewise constant $r = 0$ and piecewise linear $r = 1$ signals. As the PRUTF algorithm detects more change points and forms the augmented boundary set \mathcal{A} , the local minima or maxima corresponding to these change points are removed from the stochastic process

$$\hat{u}_{-\mathcal{A}}^{\text{st}}(t) = \left[(\mathbf{D}_{-\mathcal{A}} \mathbf{D}_{-\mathcal{A}}^T)^{-1} \mathbf{D}_{-\mathcal{A}} \right]_t \mathbf{y} = \sum_{j=0}^J \hat{u}_j^{\text{st}}(t) \mathbb{1}\{t \in B_j\}, \quad (31)$$

for $t = 1, \dots, m - |\mathcal{A}|$. This fact is shown by olive-colored lines (—) in Figure 4. The last equality in (31) expresses that the $\hat{u}_{-\mathcal{A}}^{\text{st}}(t)$ is the stochastic term of the dual variables for all the interior coordinates and is derived by stacking the stochastic terms of the dual variables associated with j -th block, $\hat{u}_j^{\text{st}}(t)$, as defined in (23), for $j = 0, \dots, J$. This behaviour suggests a way to introduce a stopping rule for the PRUTF algorithm. As can be viewed from the orange-colored lines (—) of Figure 4, if all true change points are captured by the algorithm and stored in the augmented set \mathcal{A}_0 , the resulting process

$$\hat{u}_{-\mathcal{A}_0}^{\text{st}}(t) = \left[(\mathbf{D}_{-\mathcal{A}_0} \mathbf{D}_{-\mathcal{A}_0}^T)^{-1} \mathbf{D}_{-\mathcal{A}_0} \right]_t \mathbf{y} \quad \text{for } t = 0, \dots, m - |\mathcal{A}_0|,$$



(a) Piecewise constant with $r = 0$

(b) Piecewise linear with $r = 1$

Figure 4: The cyan-colored lines show the dual variables for the full matrix \mathbf{D} . Dual variables computed after removing rows of the matrix \mathbf{D} associated with τ_1 , that is $\mathbf{D}_{-\mathcal{A}_1}$, are displayed by the olive-colored lines. The augmented boundary set \mathcal{A}_2 corresponding to τ_1 and τ_2 results to the dual variables shown by orange-colored lines.

contains no noticeable optimum points and tends to fluctuate close to the zero line (x-axis).

We terminate the search in Algorithm 1 at step j by checking whether the maximum of $|\hat{u}_{-\mathcal{A}_j}^{\text{st}}(t)|$, for $t = 0, \dots, m - |\mathcal{A}_j|$, is smaller than a certain threshold. To exactly specify this threshold, as suggested by Theorem 1, we need to calculate the *excursion probabilities* of a Gaussian bridge process. As stated in Adler and Taylor (2009), analytic formulas for the excursion probabilities are known to be available only for a small number of Gaussian processes. One of such Gaussian processes is the Brownian bridge process. It is well known that for the Brownian bridge process $B_0(t)$ defined on the interval $[a, b]$

$$\Pr\left(\sup_{a \leq t \leq b} |B_0(t)| \geq x\right) = 2 \sum_{i=1}^{\infty} (-1)^{i+1} \exp\left(\frac{-2i^2 x^2}{b-a}\right). \quad (32)$$

See, for example, Adler and Taylor (2009), and Shorack and Wellner (2009). Hence for the piecewise constant signals, the required threshold for stopping Algorithm 1 can be obtained from (32), for a suitably chosen interval $[a, b]$. That is, for a given value α , we choose x_α such that $\Pr(\sup_{a \leq t \leq b} |B_0(t)| \geq x_\alpha) = 1 - \alpha$. Therefore, for $r = 0$ and $a = 0, b = 1$, we stop Algorithm 1 at the iteration j_0 if

$$\max_{0 \leq t \leq 1} \left| \hat{\mathbf{u}}_{-\mathcal{A}_{j_0}}^{\text{st}}(\lfloor kt \rfloor) \right| \leq \sigma x_\alpha \sqrt{k}, \quad \text{for } t = 0, \dots, m - |\mathcal{A}_{j_0}|,$$

and $k = m - |\mathcal{A}_{j_0}|$.

For $r \geq 1$, the threshold is obtained in a similar fashion. Although the excursion probabilities for the Gaussian bridge processes are not known, we notice that by adopting the steps for the proof of (32) in [Beghin and Orsingher \(1999\)](#), we can establish a similar formula for the Gaussian bridge process $G_0(t)$ in [Theorem 1](#) as

$$\Pr \left(\sup_{a \leq t \leq b} |G_0(t)| \geq x \right) = 2 \sum_{i=1}^{\infty} (-1)^{i+1} \exp \left(\frac{-2i^2 x^2}{S_r^2(k)} \right), \quad (33)$$

where $k = m - |\mathcal{A}_{j_0}|$, and the quantity $S_r^2(k)$ is the k -th diagonal element of the matrix

$$\left(\mathbf{D}_{-\mathcal{A}_{j_0}} \mathbf{D}_{-\mathcal{A}_{j_0}}^T \right)^{-1}.$$

Hence, we stop [Algorithm 1](#) at the iteration j_0 if

$$\max_{0 \leq t \leq 1} \left| \hat{\mathbf{u}}_{-\mathcal{A}_{j_0}}^{\text{st}}(\lfloor kt \rfloor) \right| \leq \sigma x_\alpha (k-r)^{(2r+1)/2}, \quad \text{for } t = 0, \dots, m - |\mathcal{A}_{j_0}|, \quad (34)$$

where x_α is derived from the equation

$$\sum_{i=1}^{\infty} (-1)^{i+1} \exp \left(\frac{-2i^2 x_\alpha^2}{S_r^2(k)} \right) = \frac{\alpha}{2}. \quad (35)$$

6 Pattern Recovery and Theories

The main purpose of this section is to investigate whether the PRUTF algorithm can recover features of the true signal \mathbf{f} . We also demonstrate conditions under which the structure of the estimated signal $\hat{\mathbf{f}}$ matches the true signal \mathbf{f} . To verify the performance of PRUTF in the discovery the true signal, we first define what we mean by pattern recovery.

Definition 1 (*Pattern Recovery*): A trend filtering estimate $\hat{\mathbf{f}}$ recovers the pattern of the true signal \mathbf{f} if

$$\text{sign}([\mathbf{D}\hat{\mathbf{f}}]_i) = \text{sign}([\mathbf{D}\mathbf{f}]_i), \quad \text{for } i = 1, \dots, m, \quad (36)$$

where $m = n - r - 1$ is the number of rows of matrix \mathbf{D} . We use the notation $\hat{\mathbf{f}} \stackrel{pr}{=} \mathbf{f}$ to briefly denote the pattern recovery feature of $\hat{\mathbf{f}}$.

In the asymptotic framework, a trend filtering estimate is called pattern consistent if

$$\Pr(\hat{\mathbf{f}} \stackrel{pr}{=} \mathbf{f}) \rightarrow 1 \quad \text{as } n \rightarrow \infty, \quad (37)$$

where $\hat{\mathbf{f}} = \hat{\mathbf{f}}_n$, to denote its dependency to the sample size n . Pattern recovery is very similar to the concept of sign recovery in lasso ([Zhao and Yu, 2006](#); [Wainwright, 2009](#)) as it deals with the specification of both locations of non-zero coefficients and their signs.

The problem of pattern recovery is studied for the special case of the fused lasso in several papers. [Rinaldo et al. \(2009\)](#) derived conditions under which fused lasso consistently identifies the true pattern. This was contradicted by [Rojas and Wahlberg \(2014\)](#), who argued that fused lasso does not always succeed in discovering the exact change points. [Rojas and Wahlberg](#)

(2014) showed that fused lasso can be reformulated as the usual lasso, for which the necessary conditions for exact sign recovery have been established in the literature. Then, they proved that one such necessary condition, known as the irrepresentable condition, is not satisfied for the transformed lasso when there is a specific pattern called a staircase (Definition 2). Corrections to Rinaldo et al. (2009) were appeared in Rinaldo (2014). Later on, Qian and Jia (2016) proposed a method called puffer transformation, which is shown to be consistent in specifying the exact change points, including in the presence of staircases.

In the remaining part of this section, we use the dual variables to demonstrate the situations in which PRUTF can correctly recover the pattern of the true signal. Exact pattern recovery implies that the dual variables are comprised of $J_0 + 1$ consecutive bounded processes whose endpoints correspond to the true change points. The following lemma describes the situations in which exact pattern recovery can be attained. A particular case of this result in the context of piecewise constant signals was established in Rinaldo (2014).

Theorem 2 *Exact pattern recovery in PRUTF occurs when the discrete time processes $\{\hat{u}_j^{\text{st}}(t), t = \tau_j + r_a, \dots, \tau_{j+1} - r_b\}$, for $j = 0, \dots, J_0$, satisfy the following conditions simultaneously with probability one:*

(a) **First block constraint:** for $t = 1, \dots, \tau_1 - r_b$,

$$-\lambda \left(1 - [(\mathbf{D}_{-A} \mathbf{D}_{-A}^T)^{-1} \mathbf{D}_{-A}]_t \mathbf{D}_{A_1}^T \mathbf{1}\right) \leq \hat{u}_0^{\text{st}}(t) \leq \lambda \left(1 + [(\mathbf{D}_{-A} \mathbf{D}_{-A}^T)^{-1} \mathbf{D}_{-A}]_t \mathbf{D}_{A_1}^T \mathbf{1}\right). \quad (38)$$

(b) **Last Block constraint:** for $t = \tau_{J_0} + r_a, \dots, m$,

$$-\lambda \left(1 + [(\mathbf{D}_{-A} \mathbf{D}_{-A}^T)^{-1} \mathbf{D}_{-A}]_t \mathbf{D}_{A_{J_0}}^T \mathbf{1}\right) \leq \hat{u}_{J_0}^{\text{st}}(t) \leq \lambda \left(1 - [(\mathbf{D}_{-A} \mathbf{D}_{-A}^T)^{-1} \mathbf{D}_{-A}]_t \mathbf{D}_{A_{J_0}}^T \mathbf{1}\right). \quad (39)$$

(c) **Interior Block constraints:** for $t = \tau_j + r_a, \dots, \tau_{j+1} - r_b$, if $s_j \neq s_{j+1}$

$$\begin{aligned} -\lambda \left(1 - [(\mathbf{D}_{-A} \mathbf{D}_{-A}^T)^{-1} \mathbf{D}_{-A}]_t (\mathbf{D}_{A_{j+1}}^T \mathbf{1} - \mathbf{D}_{A_j}^T \mathbf{1})\right) &\leq \hat{u}_j^{\text{st}}(t) \\ &\leq \lambda \left(1 + [(\mathbf{D}_{-A} \mathbf{D}_{-A}^T)^{-1} \mathbf{D}_{-A}]_t (\mathbf{D}_{A_{j+1}}^T \mathbf{1} - \mathbf{D}_{A_j}^T \mathbf{1})\right), \end{aligned} \quad (40)$$

and if $s_j = s_{j+1}$, which corresponds to a staircase block, $\hat{u}_j^{\text{st}}(t) \leq 0$ or $\hat{u}_j^{\text{st}}(t) \geq 0$.

In the foregoing equations, $\mathbf{1} \in \mathbb{R}^{r+1}$ is a vector of size $r + 1$ whose elements are all 1. A proof of the theorem is given in Appendix A.2.

We analyze the performance of the PRUTF algorithm in pattern recovery in two different scenarios; signals with staircase patterns and signals without staircase patterns. To our knowledge, Rojas and Wahlberg (2014) was the first paper to carefully investigate the staircase pattern for the piecewise constant signals in the change points analysis setting. In Rojas and Wahlberg (2014), a staircase pattern for a piecewise constant signal refers to the phenomenon of equal signs in two consecutive changes. We extend this concept to the general case, which covers any piecewise polynomial signals of order r , by applying the penalty matrix $\mathbf{D} = \mathbf{D}^{(r+1)}$.

Definition 2 *Suppose that the true signal \mathbf{f} is a piecewise polynomial of order r with change points at the locations $\boldsymbol{\tau} = \{\tau_1, \dots, \tau_{J_0}\}$. Moreover, let $\mathbf{B} = \{B_0, \dots, B_{J_0}\}$ be blocks created by the change points in $\boldsymbol{\tau}$. A staircase occurs in block B_j , $j = 1, \dots, J_0 - 1$ if*

$$\text{sign}([\mathbf{D}\mathbf{f}]_{\tau_j}) = \text{sign}([\mathbf{D}\mathbf{f}]_{\tau_{j+1}}). \quad (41)$$

The following theorem investigates the consistency of PRUTF in pattern recovery, in both with and without staircases. Specifically, it shows that for a signal without a staircase, the exact pattern recovery conditions are satisfied with probability one. On the other hand, in the presence of staircases in the signal, the probability of these conditions holding, which is equivalent to the probability of a Gaussian bridge process never crossing the zero line, converges to zero.

In the literature, the consistency of a change point method is usually characterized by the signal size n , the number of change points J_0 , the noise variance σ_n^2 , the minimal spacing between change points,

$$\underline{L}_n = \min_{j=0, \dots, J_0} |L_{n,j}| = \min_{j=0, \dots, J_0} |\tau_{j+1} - \tau_j|,$$

and the minimum magnitude of jumps between change points,

$$\delta_n = \min_{j=1, \dots, J_0} |\mathbf{D}_{\tau_j} \mathbf{f}|.$$

All the above quantities are allowed to change as n grows.

In the following, we present our main theorem providing conditions under which the output of the PRUTF algorithm consistently recovers the pattern of the true signal \mathbf{f} .

Theorem 3 *Suppose that \mathbf{y} follows the model in (1). Let $\boldsymbol{\tau}$ be the set of J_0 change points for the true signal \mathbf{f} . Additionally, assume that $\hat{\boldsymbol{\tau}}_n$ and $\hat{\mathbf{f}}_n$ are the set of change points estimates and the corresponding signal estimate obtained by the PRUTF algorithm, respectively. The followings hold for the PRUTF algorithm.*

(a) **Non-staircase Blocks:** *Suppose there is no staircase block in the true signal \mathbf{f} . For some $\xi > 0$ and with*

$$\lambda_n < \frac{\delta_n \underline{L}_n^{2r+1}}{n^{2r} 2^{r+2}},$$

if the conditions

$$\bullet \quad \frac{\delta_n \underline{L}_n^{r+1/2}}{n^r \sigma_n} \rightarrow \infty \quad \text{and} \quad \frac{\delta_n \underline{L}_n^{r+1/2}}{2^{r/2+2} n^r \sigma_n \sqrt{\log(J_0)}} > (1 + \xi), \quad (42)$$

$$\bullet \quad \frac{\lambda_n \underline{L}_n^{r+1/2}}{n^r \sigma_n} \rightarrow \infty \quad \text{and} \quad \frac{2^{r/2+1} \lambda_n \underline{L}_n^{r+1/2}}{n^r \sigma_n \sqrt{\log(n - J_0)}} > (1 + \xi), \quad (43)$$

hold, then the PRUTF algorithm guarantees exact pattern recovery with probability approaching one. That is,

$$\Pr(\hat{\mathbf{f}}_n \stackrel{pr}{=} \mathbf{f}) \rightarrow 1 \quad \text{as} \quad n \rightarrow \infty.$$

(b) **Staircase Blocks:** *On the other hand, if the true signal \mathbf{f} contains at least one staircase block, then the probability of exact pattern recovery by the PRUTF algorithm converges to zero. That is,*

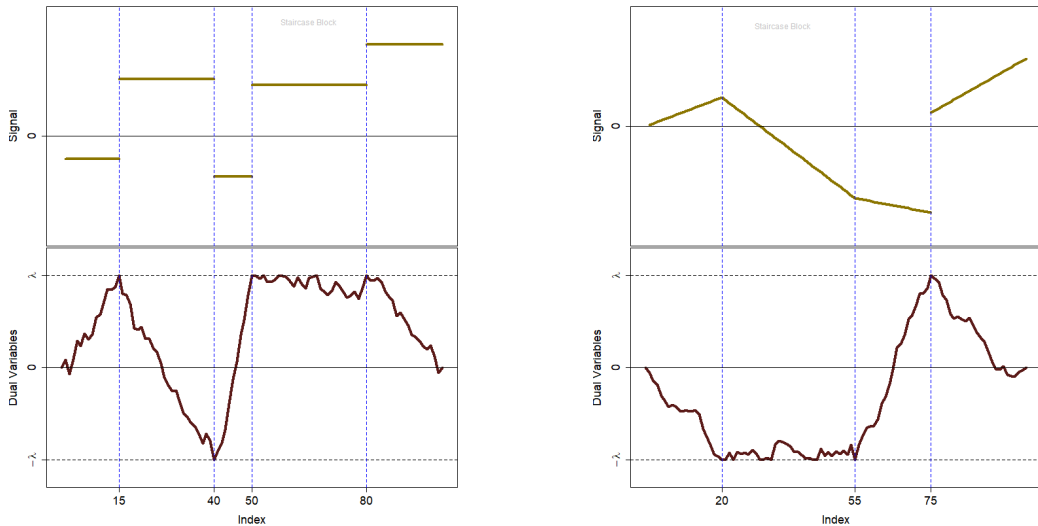
$$\Pr(\hat{\mathbf{f}}_n \stackrel{pr}{=} \mathbf{f}) \rightarrow 0 \quad \text{as} \quad n \rightarrow \infty.$$

A proof is given in Appendix A.3.

Remark 7 The performance of PRUTF in terms of consistent pattern recovery relies on the quantity $\delta_n \underline{L}_n^{r+1/2}/\sigma_n$ and the choice of λ_n . In the piecewise constant case, the former quantity reduces to the well-known signal-to-noise-ratio quantity, which is crucial for a consistent change point estimation (Fryzlewicz et al., 2014; Wang et al., 2020). The statements in 42 illustrate that the consistency of PRUTF in non-staircase blocks is achievable if the quantity $\delta_n \underline{L}_n^{r+1/2}/\sigma_n$ is of order $O(n^{r+c})$, for some $c > 0$. In addition, the number of the change points J_0 is allowed to diverge, provided

$$\log(J_0) \lesssim \frac{\delta_n^2 \underline{L}_n^{2r+1}}{n^{2r} \sigma_n^2}.$$

The drift term (24) plays a key role in assessing the performance of PRUTF in pattern recovery. From (18), this drift for a staircase block B_j becomes λs_j , which is constant in t for the entire block. Consequently, the interior dual variables $\hat{u}_j(t; \lambda)$ for the staircase block B_j contain only the stochastic term $\hat{u}_j^{\text{st}}(t) = \left[(\mathbf{D}_{-A} \mathbf{D}_{-A}^T)^{-1} \mathbf{D}_{-A} \right]_t \mathbf{y}$, which fluctuates around the line λs_j . Recall that the KKT conditions for the dual problem of trend filtering require $\hat{u}_j(t; \lambda)$ to stay within the lines $-\lambda$ and λ . Thus, for a signal with staircase patterns, the PRUTF algorithm is sensitive to the variability of random noises and identifies change points once $\hat{u}_j^{\text{st}}(t)$ touches the $\pm\lambda$ boundaries. Examples of piecewise constant and piecewise linear signals, along with their corresponding dual variables, are depicted in Figure 5, in which the above argument can be clearly seen.



(a) Piecewise constant signal with staircase block (50, 80].

(b) Piecewise linear signal with staircase block (20, 55].

Figure 5: Piecewise constant and piecewise linear signals with staircase pattern at blocks (50, 80] and (20, 55] and their corresponding dual variables.

According to Theorem 3, if there is no staircase pattern in the underlying signal, the PRUTF algorithm consistently estimates the true signal, and fails to do so, otherwise. Given the results

in Theorem 3, the natural question is whether Algorithm 1 could be modified to enjoy the consistent pattern recovery in any case. In the next section, we will present an effective remedy based on altering the sign of a change associated with a staircase block.

7 Modified PRUTF Algorithm

In this section, we attempt to modify the PRUTF algorithm in such a way that it produces consistent estimates of the number and locations of change points even in the presence of staircase patterns. As previously mentioned, for a staircase block, the drift term (24) is constant and leads to false discoveries in change points. This is shown in Figure 6 with a piecewise constant signal of size $n = 100$ and the true change points at $\tau = \{15, 40, 50, 80\}$. The figure reveals that the staircase block $(50, 80]$ leads to three false discoveries at the locations 52, 54 and 76.

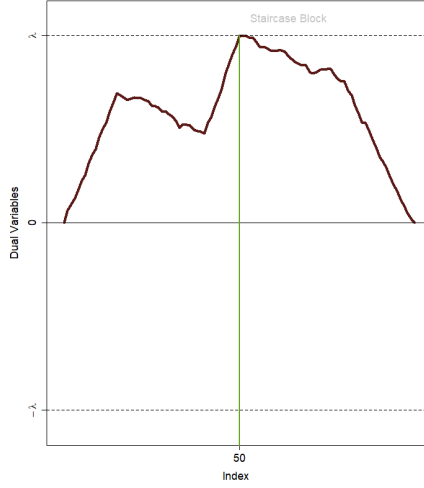
The inconsistency of PRUTF in the presence of a staircase as established in Theorem 3, stems from the fact that the change signs of the two consecutive change points at both ends of the staircase block are identical. That is, for the staircase block B_j , $\text{sign}([\mathbf{Df}]_{\tau_j}) = \text{sign}([\mathbf{Df}]_{\tau_{j+1}})$. Therefore, a question arises: can we modify Algorithm 1 in such a way that the change signs of two neighbouring change points never become equal but still yield the solution path of trend filtering? We suggest a simple but very efficient solution to the above question.

Once a new change point is identified, we check whether its r -th order difference sign is the same as that of the change points right before and after. If these change signs are not identical, then the procedure continues to search for the next change point. Otherwise, we replace the sign of the neighbouring change point with zero. This replacement of the sign prevents the drift term (24) from becoming zero. This idea is implemented for the above signal, and the result is displayed in Figure 7. As shown in panel (b), the sign of the first change point at location 50 is set to zero since its sign is identical to the sign of the second change point at 15. This sign replacement vanishes false discoveries appeared in panel (b) of Figure 6.

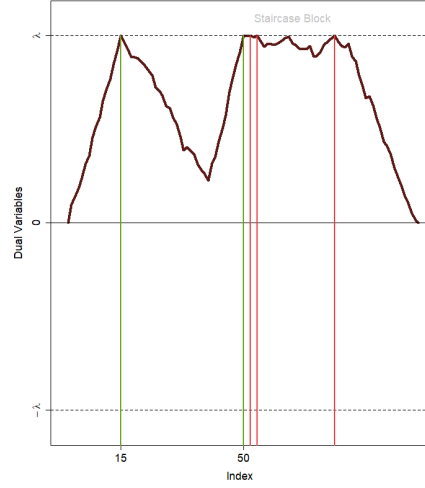
Based on the above argument, PRUTF presented in Algorithm 1 can be modified as follows to avoid false discovery and to produce consistent pattern recovery.

Algorithm 2 (mPRUTF)

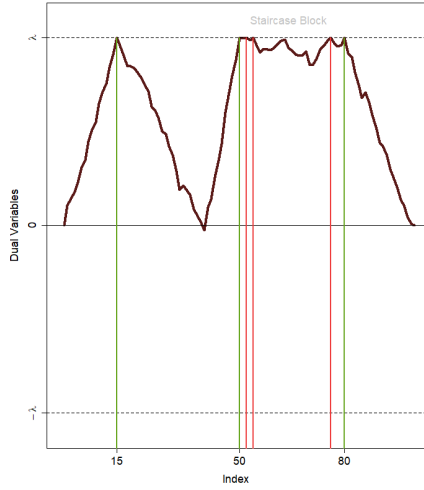
1. *Execute steps 1 and 2 of Algorithm 1.*
2. (a) *Execute part (a) of step 3 in Algorithm 1 to obtain τ_j^{join} and its sign s_j^{join} . At this point, the algorithm checks whether s_j^{join} is identical to the signs of the change points just before and after τ_j^{join} . If so, set the sign of change point which is identical to s_j^{join} to zero. Then, repeat part (a) of step 3 again to obtain new τ_j^{join} and s_j^{join} and update the sets \mathcal{A}_j and \mathcal{B}_j .*
 - (b) *Execute parts (b) and (c) of step 3 in Algorithm 1.*
3. *Repeat step 3 until either $\lambda_j > 0$ or a stopping rule is met.*



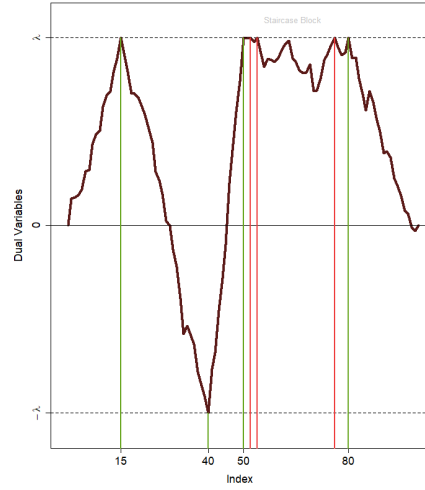
(a) First change point at $\tau = 50$.



(b) Second change point at $\tau = 15$.



(c) Third change point at $\tau = 80$.



(d) Fourth change point at $\tau = 40$.

Figure 6: The process of detecting change points using PRUTF for a signal with a staircase pattern. In panel (b), there are three falsely detected change points $\{52, 54, 76\}$ which is due to the staircase block $(50, 80]$.

The modified PRUTF (mPRUTF) algorithm produces consistent change point estimations, even in the presence of staircase patterns. This consistency has been achieved by converting the staircase patterns to non-staircase patterns that avoid false change point detection. In other words, running mPRUTF on an arbitrary signal (with or without staircases) is equivalent to running PRUTF on a signal without any staircase; see Figures 6 and 7. Thus, from part (a) of Theorem 3, the mPRUTF algorithm is consistent in pattern recovery.

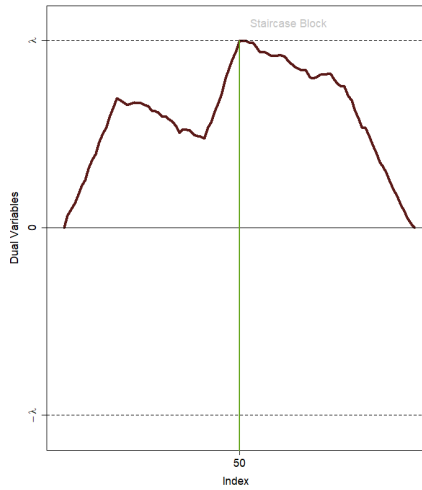
Remark 8 In step 2, part (a) of the mPRUTF algorithm, presented in Algorithm 2, it is impossible for the sign s_j^{join} of the new change point to be identical to the sign of both of its immediate neighbouring change points, because the algorithm has already checked the equality of

signs at previous steps. If they are equal, the sign of the immediate neighbouring change point will be set to zero.

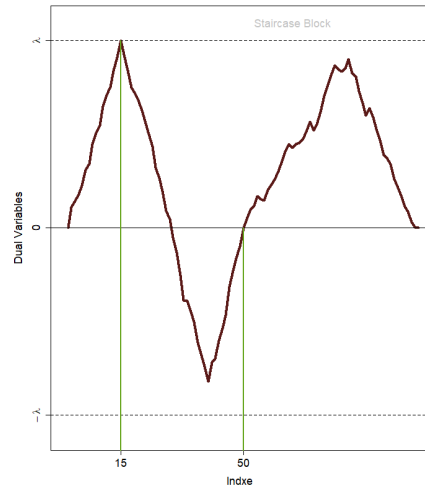
Recall that the KKT optimality conditions for solutions of the trend filtering problem in (5) requires the dual variables $\hat{\mathbf{u}}_\lambda$ to be less than or equal to λ in absolute values, i.e., $|\hat{\mathbf{u}}_\lambda| \leq \lambda$. This condition still holds when we replace the sign values (+1 or -1) with 0. Consequently, we have the following theorem.

Theorem 4 *The mPRUTF algorithm presented in Algorithm 2 is a solution path of trend filtering.*

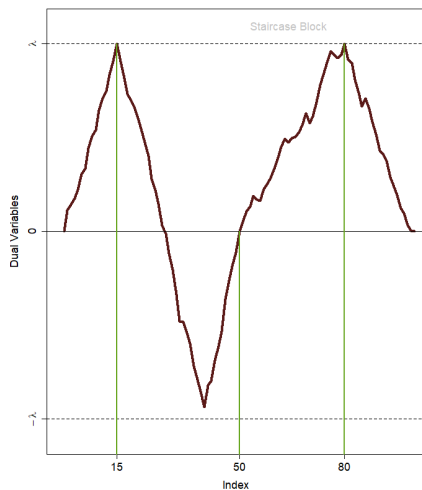
For brevity, we do not provide the proof of Theorem 4 here. We refer the reader to the similar arguments for the LARS algorithm of lasso in Tibshirani et al. (2013).



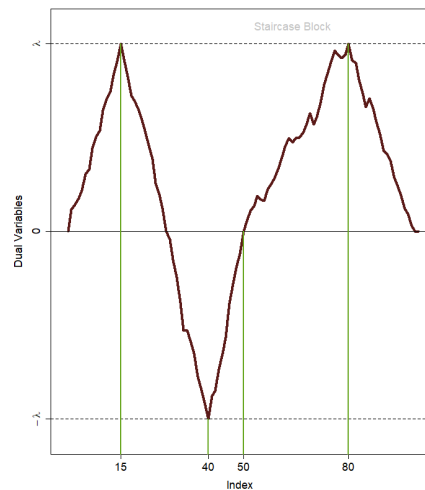
(a) First change point at $\tau = 50$.



(b) Second change point at $\tau = 15$.



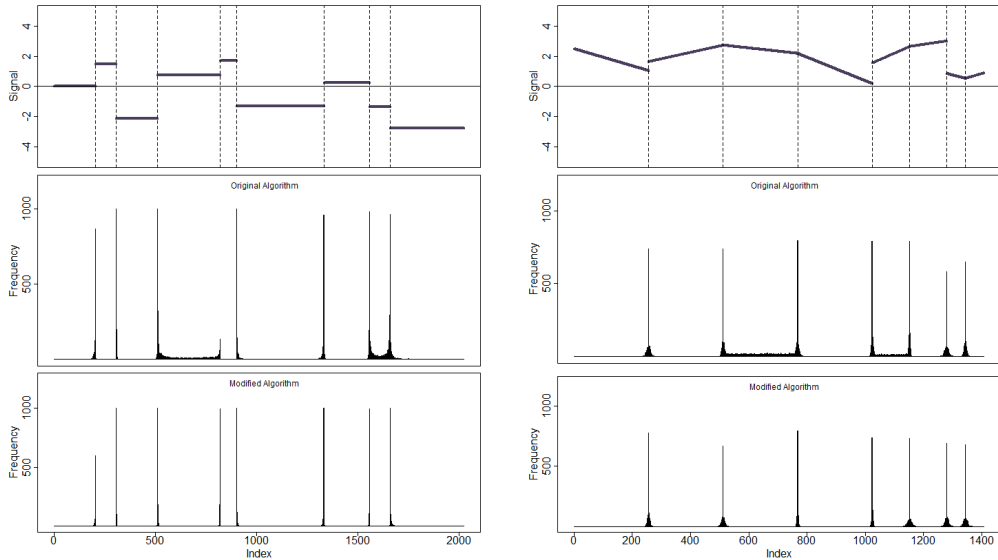
(c) Third change point at $\tau = 80$.



(d) Fourth change point at $\tau = 40$.

Figure 7: Steps of the mPRUTF algorithm until all four true change points are identified.

It is worth pointing out that the mPRUTF algorithm requires slightly more computation than the original PRUTF algorithm. The increase in computation time directly depends on the number of staircase blocks in the underlying signal. To show how mPRUTF resolves the problem of false discovery in signals with staircases, we ran both algorithms for 1000 generated datasets from a piecewise constant and piecewise linear signals. The frequency plot of the estimated change points for both algorithms are represented in Figure 8. The figure reveals that the original algorithm produces false discoveries within staircase blocks for both signals, whereas mPRUTF resolves this issue.



(a) A piecewise constant signal with blocks 4 and 8 as staircase blocks. (b) A piecewise linear signal with blocks 3 and 5 as staircase blocks.

Figure 8: The frequency plots of estimated change points using the PRUTF and mPRUTF algorithms.

8 Numerical Studies

In this section, we provide numerical studies to demonstrate the effectiveness and performance of our proposed algorithm, mPRUTF. We begin with a simulation study and then provide real data analyses.

8.1 Simulation Study

In this section, we investigate the performance of our proposed method, mPRUTF, by a simulation study. We consider two scenarios, namely piecewise constant and piecewise linear signals with staircase patterns. We compare our method to some powerful state-of-the-art approaches in change point analysis. These methods, a list of their available packages on CRAN, and their applicability for different scenarios are listed in Table 1.

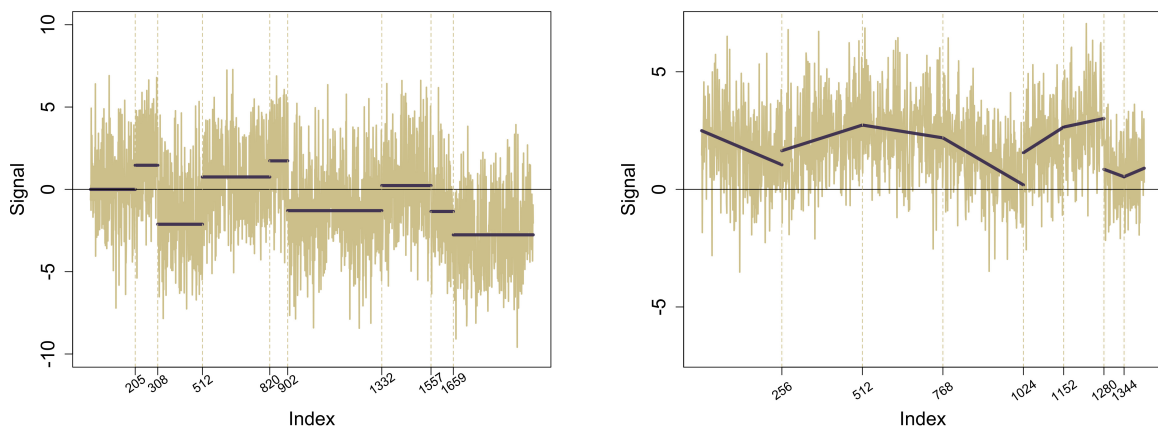
Method	Reference	R Package	Signal	
			PWC	PWL
PELT	Killick et al. (2012)	changepoint	✓	✗
WBS	Fryzlewicz et al. (2014)	wbs	✓	✗
SMUCE	Frick et al. (2014)	stepR	✓	✗
NOT	Baranowski et al. (2019)	not	✓	✓
ID	Anastasiou and Fryzlewicz (2019)	IDetect	✓	✓

Table 1: A list of change point detection and estimation methods with their packages in CRAN. The last two columns indicate which methods can be applied to piecewise constant or/and piecewise linear signals.

We have adopted the simulation setting of [Baranowski et al. \(2019\)](#), and consider piecewise constant and piecewise linear signals as follows.

- (i) A piecewise constant signal (PWC) of size $n = 2024$ with the number of change points $J_0 = 8$. The locations of the true change points are $\tau = \{205, 308, 512, 820, 902, 1332, 1557, 1659\}$ with jump sizes 1.464, -0.656, 0.098, 1.830, 0.537, 0.768, -0.574, -3.335. We set the starting intercept to 0.
- (ii) A piecewise linear signal (PWL) of size $n = 1408$ and the number of change points $J_0 = 7$. The true change points are located at $\tau = \{256, 512, 768, 1024, 1152, 1280, 1344\}$. The corresponding intercepts and slopes for 8 created blocks by τ are 0.111, 0.553, -0.481, 3.002, -7.169, -0.030, 7.217, -0.958 and -8, 6, -3, -11, 12, 4, -7, 8, respectively.

Figure 9 displays the true PWC and PWL signals, with their representative datasets generated



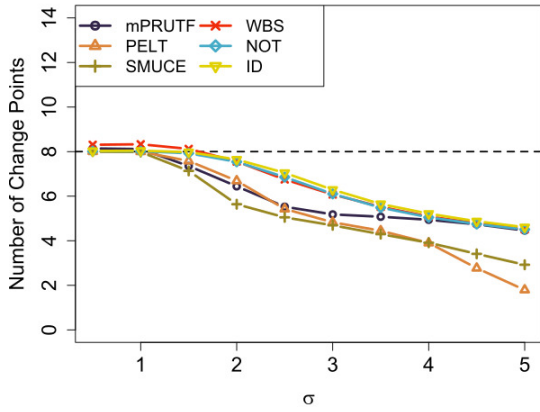
(a) PWC signal with staircases at blocks (512, 820] and (1557, 1659]. (b) PWL signal with staircases at blocks (512, 768] and (1024, 1152].

Figure 9: The piecewise constant (PWC) and piecewise linear (PWL) signals with the generated samples used in the simulation study.

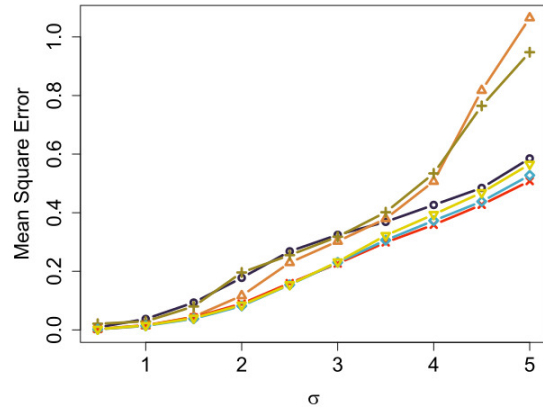
using model (1). We note that both PWC and PWL signals contain two staircase blocks. These blocks for the PWC signal are (512, 820], (1557, 1659] and for PWL signal are (512, 768] and (1024, 1152].

We apply mPRUTF presented in Algorithm 2 to estimate the number and the locations of the change points for the PWC and PWL signals. In each iteration of the simulation study, we simulate a dataset according to model (1) under the assumption that the error terms are independently and identically distributed as $N(0, \sigma^2)$. Moreover, we set the significance level to $\alpha = 0.05$ for the stopping rule in (34).

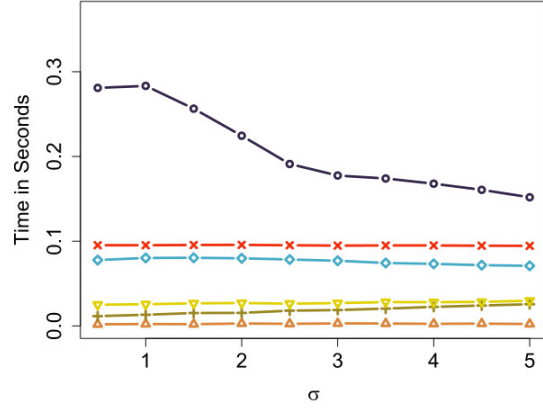
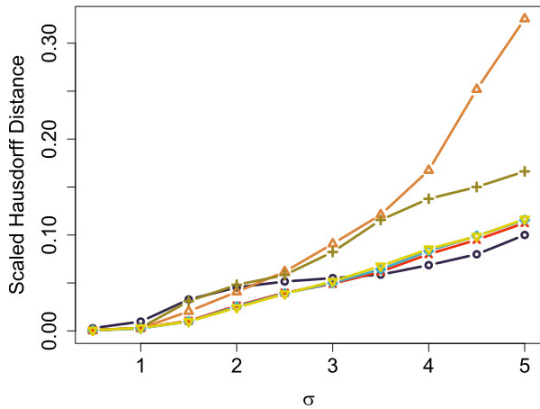
In order to explore the impact of different noise levels on the change point methods, we run each simulation for various values of σ in $\{0.5, 1, 1.5, \dots, 4.5, 5\}$. We run the simulation $N = 5000$ times and report the results for each change point technique in terms of estimates of the



(a) Average number of change points.



(b) MSE estimations.



(c) Computation time.

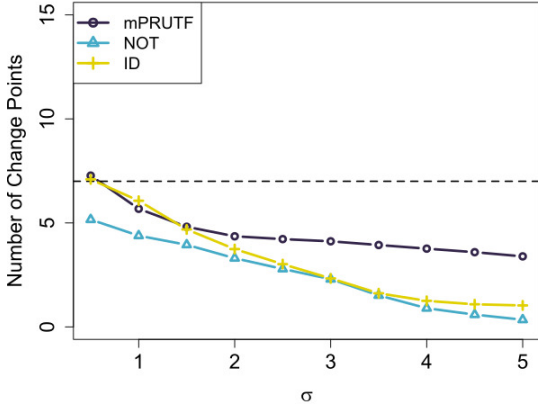
Figure 10: The estimated average number of change points, MSE and Hausdorff distance, as well as the computation time of various methods for PWC signal. The results are provided for different values of the noise variability σ .

number of change points, estimates of the mean square error given by $\text{MSE} = N^{-1} \sum_{i=1}^N (\hat{f}_i - f_i)^2$, estimates of the scaled Hausdorff distance given by

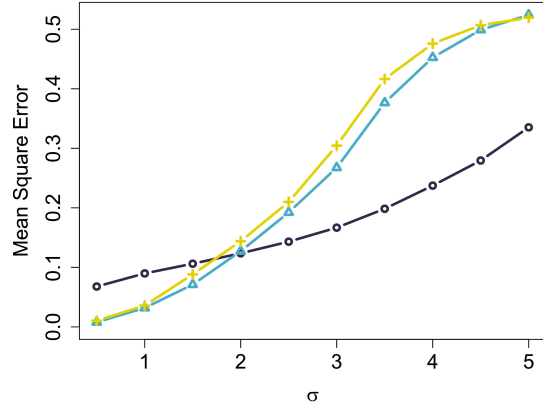
$$d_H = \frac{1}{N} \max \left\{ \max_{j=0, \dots, J_0} \min_{i=0, \dots, \hat{J}_0} |\hat{\tau}_i - \tau_j|, \max_{i=0, \dots, \hat{J}_0} \min_{j=0, \dots, J_0} |\hat{\tau}_i - \tau_j| \right\},$$

and the computation time in seconds. These quantities are frequently used to assess the performance of a change point detection technique in the literature, for example, see [Baranowski et al. \(2019\)](#), [Anastasiou and Fryzlewicz \(2019\)](#). The signal estimate, \hat{f} , is computed by the least square fit of a polynomial of order r to the observations within segments created by each change point method. We also remark that the tuning parameters and stopping criteria for the methods listed in [Table 1](#) are set to the default values by the packages.

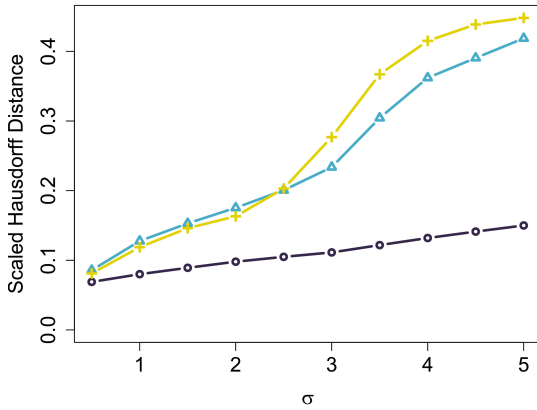
The results for the PWC and PWL signals are presented in [Figures 10 and 11](#), respectively.



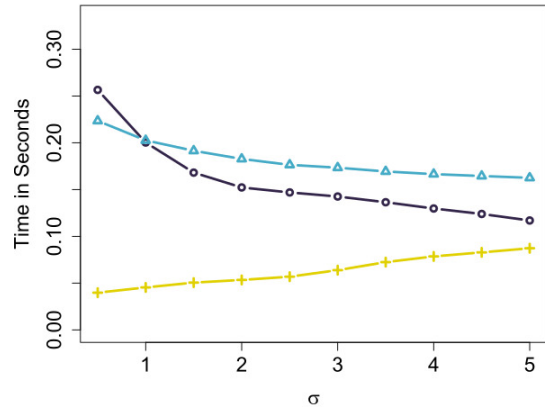
(a) Average number of change points.



(b) MSE estimations



(c) Hausdorff distance.



(d) Computation time.

Figure 11: The estimated average number of change points, MSE and Hausdorff distance, as well as the computation time of various methods for PWL signal. The results are provided for different values of the noise variability σ .

In the case of piecewise constant signal, as in Figure 10, mPRUTF performs comparable to PELT and SMUCE in terms of the average number of change points, MSE and the scaled Hausdorff distance up to $\sigma = 3$, and outperforms them as σ increases. For $\sigma \geq 4$, similar performance to WBS, NOT and ID is viewed from these measurements. As indicated by the average number of change points, MSE and the scaled Hausdorff distance, WBS, NOT and ID outperform the other methods in almost all noise levels. From a computational point of view, mPRUTF takes a slightly longer time, mainly due to the matrix \mathbf{D} multiplications, however, this computation time decreases as noise level σ increases. As in panel (d) of Figure 10, the methods PELT, SMUCE and ID are the fastest ones.

In the case of piecewise linear signal, mPRUTF is only compared to NOT and ID methods, which are applicable to the piecewise polynomials of order $r \geq 1$. As in Figure 11 mPRUTF outperforms both NOT and ID in terms of the average number of change points and the scaled Hausdorff distance for all noise levels. In terms of MES, mPRUTF outperforms the other two for $\sigma \geq 2$. As shown in Panel (d) of Figure 11, the computation time of mPRUTF ranks second after ID.

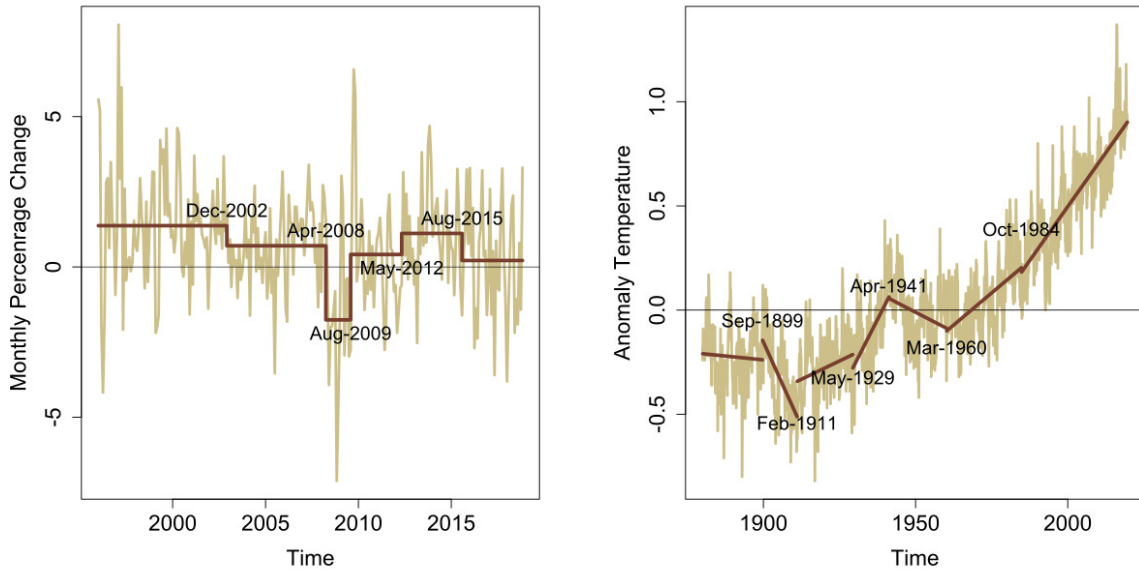
The mPRUTF method performs well in terms of the estimation of the number of change points, their locations, as well as the true signals. In fact, simulation results for most of the scenarios indicate that mPRUTF is among the most competitive change point detection approaches in the literature.

8.2 Real Data Analysis

In this section, we have analyzed UK HPI and GISTEMP and COVID-19 datasets, using our proposed algorithm. Because σ^2 is unknown for these real datasets, we applied median absolute deviation (MAD) proposed by Hampel (1974), to robustly estimate σ^2 . More specifically, a MAD estimate of σ for piecewise constant signals is given by $\hat{\sigma} = \text{Median}(\mathbf{D}^{(1)} \mathbf{y}) / [\sqrt{2} \Phi^{-1}(0.75)]$ and for piecewise linear signals by $\hat{\sigma} = \text{Median}(\mathbf{D}^{(2)} \mathbf{y}) / [\sqrt{6} \Phi^{-1}(0.75)]$, where $\Phi^{-1}(\cdot)$ represents the inverse cumulative density function of the standard normal distribution.

Example 1 (UK HPI Data) *The UK House Price Index (HPI) is a National Statistic that shows changes in the value of residential properties in England, Scotland, Wales and Northern Ireland. The HPI measures the price changes of residential housing by calculating the price of completed houses sale transactions as a percentage change from some specific start date. The UK HPI uses the hedonic regression model as a statistical approach to produce estimates of the change in house prices for each period. For more details, see <https://landregistry.data.gov.uk/app/ukhpi>. Many researchers, including Fryzlewicz (2018), Fryzlewicz et al. (2018) and Anastasiou and Fryzlewicz (2019), have studied the UK HPI dataset in carrying out change point analysis. In the current study, we consider monthly percentage changes in the UK HPI at Tower Hamlets (an east borough of London) from January 1996 to November 2018.*

We have applied the mPRUTF algorithm to the dataset. The algorithm have found five change points located at the dates December 2002, April 2008 and August 2009 (may be attributed to the Credit Crunch and Financial Crises), May 2012 (may be attributed to The London 2012



(a) UK HPI dataset and its piecewise constant fit. (b) GISTEMP dataset and its piecewise linear fit.

Figure 12: The time series and fitted signals for both Tower Hamlet HPI and GISTEMP datasets presented in examples

Summer Olympics) and August 2015 (may be attributed to regulatory and tax changes, and also by lower net migration from the EU). The dataset, the change points derived by mPRUTF and its piecewise constant fit are presented in panel (a) of Figure 12.

Example 2 (GISTEMP Data) The Goddard Institute for Space Studies (GISS) monitors broad global changes around the world. The GISS Surface Temperature Analysis (GISTEMP) is an estimate of the global surface temperature changes (see <https://www.giss.nasa.gov>). In the analysis of GISTEMP data, the temperature anomalies are used rather than the actual temperatures. A temperature anomaly is a difference from an average or baseline temperature. The baseline temperature is typically computed by averaging thirty or more years of temperature data (1951 to 1980 in the current dataset). A positive anomaly indicates the observed temperature was warmer than the baseline, while a negative anomaly indicates the observed temperature was cooler than the baseline. For more details see Hansen et al. (2010) and Lenssen et al. (2019).

The GISTEMP dataset has been frequently explored in change point literature, for example see Ruggieri (2013), James and Matteson (2015) and Baranowski et al. (2019). Panel (b) of Figure 12 displays the monthly land-ocean temperature anomalies recorded from January 1880 to August 2019 (see <https://data.giss.nasa.gov/gistemp>). The plot reveals the presence of a linear trend with several change points in the dataset. For this dataset, we have identified six change points using mPRUTF located in September 1899, February 1911, May 1929, April 1941, March 1960, October 1984. The locations of change points and an estimate of the piecewise linear signal are presented in panel (b) of Figure 12.

Example 3 (COVID-19 Data) *Since the initial outbreak of Novel Coronavirus Disease 2019 (COVID-19) in Wuhan, China, in mid-November 2019, the virus has rapidly spread throughout the world. The pandemic has infected 21.26 million people and killed more than 761,000 <https://covid19.who.int/>, greatly stressing public health systems and adversely influencing global society and economies. Therefore, every country has attempted to slow down the transmission rate by various regional and national policies such as the declaration of national emergencies, quarantines and mass testing. Of vital interest to governments is understanding the pattern of the epidemic growth and assessing the effectiveness of policies undertaken. A scientist can investigate these matters by analyzing the sequence of infection data for COVID-19. Change point detection is one possible framework for studying the behaviour of COVID-19 infection curves. By detecting the locations of alterations in the curves, change point analysis gives us insights into changes in the transmission rate or efficiency of interventions. It also enables us to raise warning signals if the disease pattern changes.*

For this example, we consider the log-scale of the cumulative number of confirmed cases for Australia, Canada, the United Kingdom and the United States, during the period March 10, 2020 through April 30, 2021. We have applied mPRUTF to detect change points that have occurred in the data for each country. We then fitted a piecewise linear model to the data using the selected change points, which provides a more direct perception of how the growth rate changes over time.

Figure 13 displays the locations of change points detected by the mPRUTF algorithm as well as the estimated linear trends for the four countries. For example, our algorithm has identified eight change points for Canada, on March 26, 2020; April 9, 2020; May 11, 2020; July 14, 2020; August 31, 2020; October 10, 2020; January 12, 2021 and March 18, 2021. The figure shows segments created by the estimated change points as well as their growth rate. The growth rate for the first segment (from March 10, 2020 to March 26, 2020) is remarkably high, but starts to slightly decline after the first change point on March 26, 2020. This mild decline may be linked to the declaration of the the state of emergency, quarantine and international travel ban declared by the Government of Canada. The third segment (from April 9, 2020 to May 11, 2020), the fourth segment (from May 11, 2020 to July 14, 2020) and the fifth segment (from July 14, 2020 to August 31, 2020) have witnessed noticeable decreases in the growth rate. The decrease can perhaps/probably be explained by the mandatory use of face-coverings and the border closure with the United States for the third segment, and the use of COVID-19 serological tests and the national contact tracing for the fourth and fifth segments. An upward trend in the growth rate observed from August 31, 2020 to October 10, 2020 could have resulted from the opening of businesses and public spaces. It seems that the second wave started on October 10, 2020, with a remarkable increase in the rate that continued until January 12, 2021. After this date, the rate again declined until March 18, 2021, which could be the result of provincial states of emergency and lockdowns. The last segment witnessed another surge in the rate, perhaps due to new variants of Coronavirus.

The mPRUTF algorithm has also detected seven change points for the United Kingdom on the following dates: April 4, 2020; April 28, 2020; May 25, 2020; June 22, 2020; September 9,

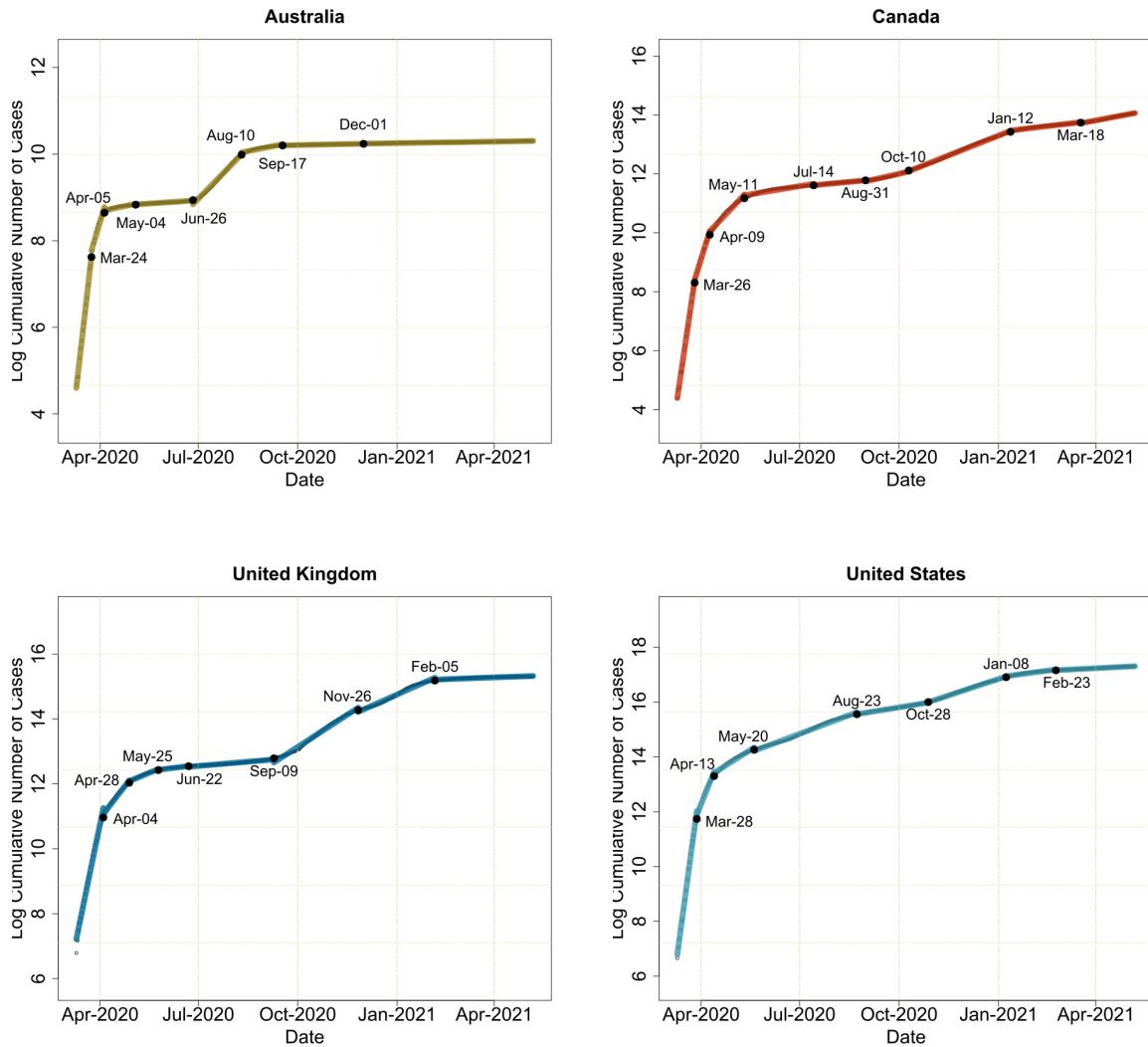


Figure 13: The change point locations and estimated linear trend for the transformed COVID-19 datasets in Example 3. The dates indicated on each plot show the detected change points.

2020; November 26, 2020 and February 5, 2021. As can be viewed from the figure, there are remarkable declines in the growth rates for the second segment (perhaps due to the nationwide lockdown), the third segment (perhaps due to the international travel ban) and the segments from May 25, 2020 to September 9, 2020 (perhaps due to mandatory use of face masks and comprehensive contact tracing). The country witnessed a significant increase in the growth rate starting from September 9, 2020, which aligns with the reopening of businesses, schools and universities. The second national lockdown could be linked to the very small decrease in the slope of the segment from November 26, 2020 to February 5, 2021. Finally, the growth rate in the last segment seemed to be under control, which could be the result of COVID vaccinations.

9 More on Models With Frequent Change Points or With Dependent Errors

This section empirically investigates the performance of mPRUTF in models with frequent change points as well as models with dependent random errors.

9.1 mPRUTF in Signals With Frequent Change Points

In order to evaluate the detection power of mPRUTF in signals with frequent change points, we employ a teeth signal for the piecewise constant case and a wave signal for the piecewise linear case. For the teeth signal, we consider a signal with 29 change points and varying segment lengths defined as follows:

- for $1 \leq t \leq 50$, $f_t = 0$ if $(t \bmod 10) \in \{1, \dots, 5\}$; $f_t = 1$, otherwise,
- for $51 \leq t \leq 150$, $f_t = 0$ if $(t \bmod 20) \in \{1, \dots, 10\}$; $f_t = 1$, otherwise,
- for $151 \leq t \leq 250$, $f_t = 0$ if $(t \bmod 40) \in \{1, \dots, 20\}$; $f_t = 1$, otherwise,
- for $251 \leq t \leq 500$, $f_t = 0$ if $(t \bmod 100) \in \{1, \dots, 50\}$; $f_t = 1$, otherwise.

The signal is displayed in the top-left panel of Figure 14. The wave signal also has 29 change points with varying slopes which is defined as follows:

- for $1 \leq t \leq 50$, $f_t = -1 + 0.4t$ if $(t \bmod 10) \in \{1, \dots, 5\}$; $f_t = 1 - 0.4t$, otherwise,

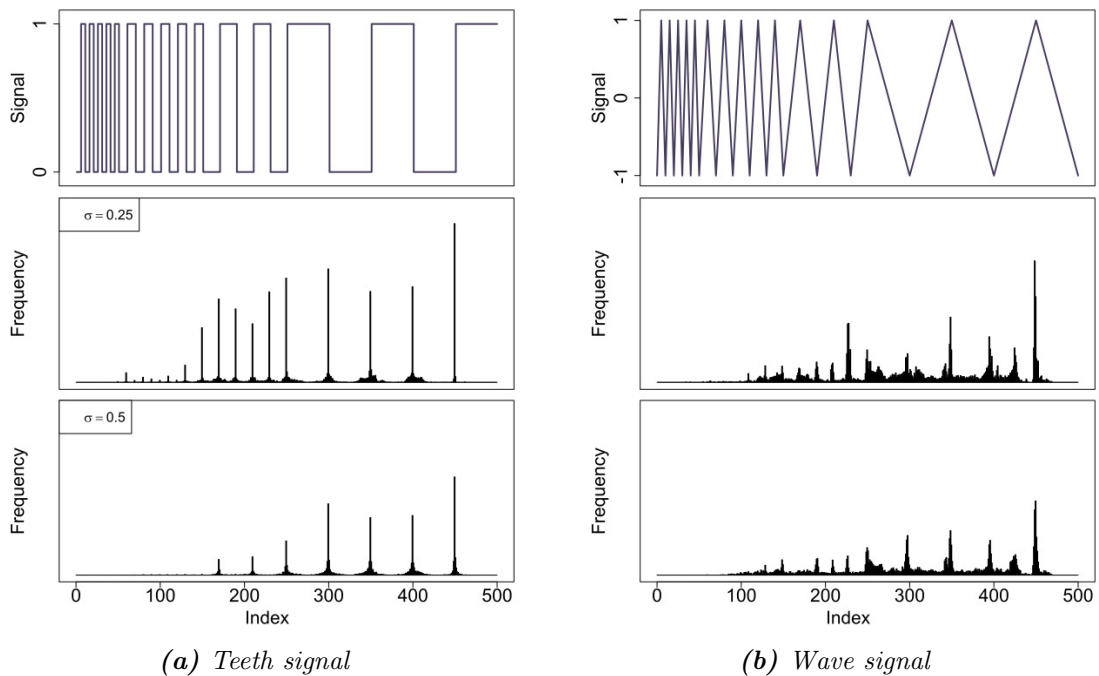


Figure 14: Histograms of the locations of change points for the teeth and wave signals. The histograms show the frequencies of the change points detected using mPRUTF in both signals. The result are displayed for two different σ values.

- for $51 \leq t \leq 150$, $f_t = -1 + 0.2t$ if $(t \bmod 20) \in \{1, \dots, 10\}$; $f_t = 1 - 0.2t$, otherwise,
- for $151 \leq t \leq 250$, $f_t = -1 + 0.1t$ if $(t \bmod 40) \in \{1, \dots, 20\}$; $f_t = 1 - 0.1t$, otherwise,
- for $251 \leq t \leq 500$, $f_t = -1 + 0.04t$ if $(t \bmod 100) \in \{1, \dots, 50\}$; $f_t = 1 - 0.04t$, otherwise.

The top-right panel of Figure 14 shows this signal.

We generated 1000 independent samples of y_t in model (1) with $\varepsilon_t \stackrel{\text{i.i.d.}}{\sim} N(0, \sigma^2)$ for both signals. The mPRUTF algorithm was then applied to these samples to estimate their change point locations. Figure 14 shows the histograms of the locations of these change points for the signals. The figure provides evidence that mPRUTF is unable to effectively detect change points in signals with frequent change points and short segments. It also shows that the results deteriorate when the noise variance σ^2 or the polynomial order r increase.

It turns out that the success of the mPRUTF algorithm critically relies on its stopping rule. Equation (34) verifies that estimating the noise variance σ^2 and specifying the threshold x_α from a Gaussian bridge process play crucial roles in the stopping rule. As discussed in Fryzlewicz (2018), the two widely used robust estimators of σ , Mean Absolute Deviation (MAD) (used here) and Inter-Quartile Range (IQR), overestimate σ in frequent change point scenarios. In addition, determining the accurate value of the threshold x_α using (35) is affected in such scenarios. These two factors prevent the stopping rule from being effective in the mPRUTF algorithm and lead to the underestimation of change points for these scenarios. We must note that such poor performance in frequent change point scenarios is not specific to mPRUTF. As investigated in Fryzlewicz (2018), state-of-the-art methods such as PELT, WBS, MOSUM, SMUCE and FDRSeg are among the approaches that fail in such scenarios.

9.2 mPRUTF in Models With Dependent Error Terms

How can mPRUTF's performance be affected by various types of random errors, such as non-Gaussian or dependent errors? This is of course an important question and will be the topic of future works. Notice that the dual solution path of trend filtering is not impacted by the type of random errors. However, the type of random errors plays a key role in the stopping rule of mPRUTF because the stopping rule is built based on Gaussian bridge processes established by Donsker's Theorem.

To empirically investigate the performance of mPRUTF for weakly dependent random errors, a simulation study is carried out here. To this end, we generate $N = 5000$ samples from model (1) with the PWC and PWL signals. We consider errors ε_i from an $AR(1)$ model with $\varepsilon_i = \rho\varepsilon_{i-1} + e_i$, for $i = 1, \dots, n$. Here, e_i 's are independent and identical random errors drawn from $N(0, (1 - \rho^2)\sigma^2)$ with $\rho \in \{-0.75, -0.5, -0.25, 0, 0.25, 0.5, 0.75\}$ and $\sigma \in \{0.5, 1, 1.5, \dots, 4.5, 5\}$. The results of mPRUTF for both PWC and PWL signals are provided in Figure 15. As can be seen, the results are very similar, in terms of the average number of change points, MSEs and the scaled Hausdorff distances, for various values of ρ . Therefore, it appears that the mPRUTF algorithm is quite robust against dependent error terms. Extensive studies of mPRUTF for non-Gaussian and dependent random errors will be carried out in future research.

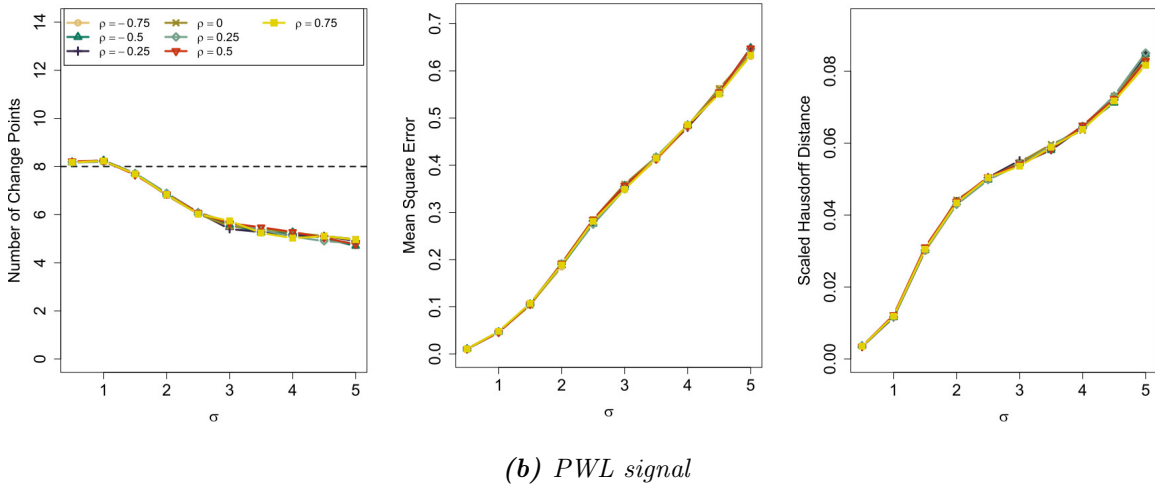
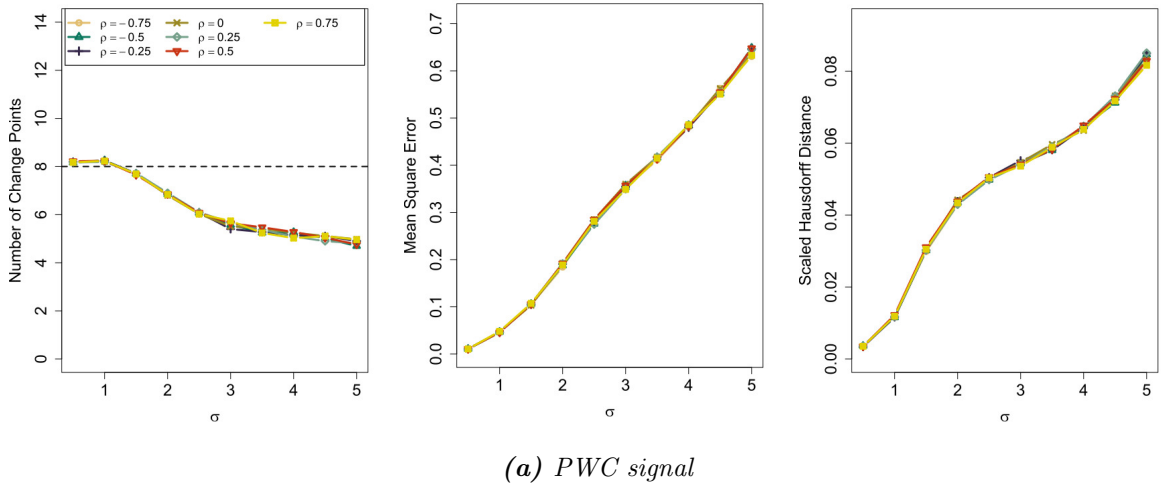


Figure 15: The estimated average number of change points, MSEs and Hausdorff distances of various methods for both PWC and PWL signals. The results are based on weakly dependent observations and provided for various values of the error variability σ .

10 Discussion

This paper proposed an algorithm, PRUTF, to detect change points in piecewise polynomial signals using trend filtering. We demonstrated that the dual solution path produced by the PRUTF algorithm forms a Gaussian bridge process for any given value of the regularization parameter λ . This conclusion allowed us to derive an efficient stopping rule for terminating the search algorithm, which is vital in change point analysis. We then proved that when there is no staircase block in the signal, the method guarantees consistent pattern recovery. However, it fails in doing so when there is a staircase in the underlying signal. To address this shortcoming in such a case, we suggested a modification in the procedure of constructing the solution path, which effectively prevents false discovery of change points. Evidence from both simulation studies and real data analysis reveals the accuracy and the high detection power of

the proposed method.

Appendix A

A.1 Proof of Theorem 1

For $\varepsilon_1, \dots, \varepsilon_n, \dots \stackrel{\text{i.i.d.}}{\sim} N(0, \sigma^2)$, and a sequence q_1, \dots, q_n, \dots of real numbers, let

$$\nu_k = \text{Var} \left(\sum_{i=1}^k q_i \varepsilon_i \right) = \sigma^2 \sum_{i=1}^k q_i^2 \quad \text{for } k \geq 1.$$

Define the partial weighted sum process $\{S_n(t) : 0 \leq t \leq 1\}$ by

$$S_n(t) = \frac{1}{\sqrt{\nu_n}} \sum_{i=1}^{\lfloor nt \rfloor} q_i \varepsilon_i, \quad \text{for } 0 \leq t \leq 1.$$

Obviously, for any $k \geq 1$, and any $0 < t_1 < t_2 < \dots < t_k \leq 1$, the vector $(S_n(t_1), \dots, S_n(t_k))$ has a multivariate normal distribution, and therefore $\{S_n(t) : 0 \leq t \leq 1\}$ is a Gaussian process for any given n .

a) In our case, first note that

$$\begin{aligned} \left[(\mathbf{D}_{-\mathcal{A}} \mathbf{D}_{-\mathcal{A}}^T)^{-1} \mathbf{D}_{-\mathcal{A}} \right]_{\lfloor mt \rfloor} \mathbf{y} &= \left[(\mathbf{D}_{-\mathcal{A}} \mathbf{D}_{-\mathcal{A}}^T)^{-1} \mathbf{D}_{-\mathcal{A}} \right]_{\lfloor mt \rfloor} (\mathbf{y} - \mathbf{f}) \\ &= \left[(\mathbf{D}_{-\mathcal{A}} \mathbf{D}_{-\mathcal{A}}^T)^{-1} \mathbf{D}_{-\mathcal{A}} \right]_{\lfloor mt \rfloor} \boldsymbol{\varepsilon}, \end{aligned} \quad (\text{A.1})$$

which is a partial weighted sum process of independent and identical Gaussian random variables ε_i , $i = 1, \dots, n$. The first equality in (A.1) is derived from the fact that the structure of the true signal \mathbf{f} remains unchanged within the j -th block, meaning that $[\mathbf{D}_{-\mathcal{A}}]_{\lfloor mt \rfloor} \mathbf{f} = 0$, for $(\tau_j + r_a)/m \leq t \leq (\tau_{j+1} - r_b)/m$, which in turn implies

$$\left[(\mathbf{D}_{-\mathcal{A}} \mathbf{D}_{-\mathcal{A}}^T)^{-1} \mathbf{D}_{-\mathcal{A}} \right]_{\lfloor mt \rfloor} \mathbf{f} = 0.$$

Thus, from the aforementioned argument for $\{S_n(t)\}$, the process $\mathbf{W}_j = \{W_j(t) : (\tau_j + r_a)/m \leq t \leq (\tau_{j+1} - r_b)/m\}$ is a Gaussian process, where

$$W_j(t) = (\tau_{j+1} - \tau_j - r)^{-(2r+1)/2} \left[(\mathbf{D}_{-\mathcal{A}} \mathbf{D}_{-\mathcal{A}}^T)^{-1} \mathbf{D}_{-\mathcal{A}} \right]_{\lfloor mt \rfloor} \mathbf{y}.$$

Additionally, with the conditions given in (26), \mathbf{W}_j is a Gaussian bridge process over the interval $(\tau_j + r_a)/m \leq t \leq (\tau_{j+1} - r_b)/m$. Furthermore, from (A.1), the mean vector and covariance matrix of \mathbf{W}_j can be computed as $\mathbf{0}$ and $\sigma^2 (\mathbf{D}_{-\mathcal{A}} \mathbf{D}_{-\mathcal{A}}^T)^{-1}$.

b) Recall that the covariance matrix $(\mathbf{D}_{-\mathcal{A}} \mathbf{D}_{-\mathcal{A}}^T)^{-1}$ is a block diagonal matrix which states that the covariance matrix between two distinct blocks is zero. This completes the proof of the theorem.

A.2 Proof of Theorem 2

- a) For $t = 1, \dots, \tau_1 - r_b$, and both signs ± 1 , according to the KKT conditions, the dual variables $\hat{u}(t)$ must lie between $-\lambda$ and λ , that is,

$$-\lambda \leq \hat{u}_0^{\text{st}}(t) - \lambda \left[(\mathbf{D}_{-\mathcal{A}} \mathbf{D}_{-\mathcal{A}}^T)^{-1} \mathbf{D}_{-\mathcal{A}} \right]_t \mathbf{D}_{A_1}^T \mathbf{1} \leq \lambda \quad (\text{A.2})$$

which yields the constraint for the first block in (38).

- b) Similar to the first block, for $t = \tau_{J_0} + r_a, \dots, m$, the constraint becomes

$$-\lambda \leq \hat{u}_{J_0}^{\text{st}}(t) + \lambda \left[(\mathbf{D}_{-\mathcal{A}} \mathbf{D}_{-\mathcal{A}}^T)^{-1} \mathbf{D}_{-\mathcal{A}} \right]_t \mathbf{D}_{A_{J_0}}^T \mathbf{1} \leq \lambda, \quad (\text{A.3})$$

which leads to the result of (39).

- c) For $t = \tau_j + r_a, \dots, \tau_{j+1} - r_b$, and $j = 1, \dots, J_0 - 1$ the constraint for the exact pattern recovery becomes

$$\lambda s_j \leq \hat{u}_j^{\text{st}}(t) - \lambda \left[(\mathbf{D}_{-\mathcal{A}} \mathbf{D}_{-\mathcal{A}}^T)^{-1} \mathbf{D}_{-\mathcal{A}} \right]_t \left(\mathbf{D}_{A_{j+1}}^T \mathbf{s}_{j+1} + \mathbf{D}_{A_j}^T \mathbf{s}_j \right) \leq \lambda s_{j+1}. \quad (\text{A.4})$$

Since the stochastic process $\hat{u}_j^{\text{st}}(t)$ is symmetric around zero, when s_{j+1} and s_j have the opposite signs, this constraint reduces to (40). Otherwise, when $s_{j+1} = s_j$, which accounts for the staircase in block j , from (18) the constraint becomes $\hat{u}_j^{\text{st}}(t) \leq 0$ or $\hat{u}_j^{\text{st}}(t) \geq 0$.

A.3 Proof of Theorem 3

- (a) The PRUTF algorithm is consistent in pattern recovery if the event

$$\left\{ \hat{\boldsymbol{\tau}} = \boldsymbol{\tau} \right\} \cap \left\{ \text{sign}(\mathbf{D}_t \hat{\mathbf{f}}_n) = \text{sign}(\mathbf{D}_t \mathbf{f}), \forall t \in \boldsymbol{\tau} \right\}, \quad (\text{A.5})$$

occurs with probability approaching one. For ease of exposition, we first compute the probability of the statement in (A.5) for the piecewise constant case, $r = 0$. We then extend this probability computation to an arbitrary piecewise polynomial $r \in \mathbb{N}$.

Case $r = 0$: In this case, the event in (A.5) is equivalent to $\{A_n \cap B_n\}$ where

$$A_n = \left\{ \min_{t \in \boldsymbol{\tau}} |\mathbf{D}_t \hat{\mathbf{f}}_n| > 0 \right\}, \quad (\text{A.6})$$

and

$$B_n = \left\{ \max_{t \in \boldsymbol{\tau}^c} |\mathbf{D}_t \bar{\boldsymbol{\epsilon}}_n| \leq 4 \lambda_n \right\}. \quad (\text{A.7})$$

For $t \in \boldsymbol{\tau}^c = \{1, \dots, m\} \setminus \boldsymbol{\tau}$, observe that $\mathbf{D}_t (\hat{\mathbf{f}}_n - \mathbf{f}) = 0$; therefore,

$$\begin{aligned} |\mathbf{D}_t \bar{\boldsymbol{\epsilon}}_n| &= |\mathbf{D}_t (\bar{\mathbf{y}}_n - \hat{\mathbf{f}}_n) + \mathbf{D}_t (\hat{\mathbf{f}}_n - \mathbf{f})| = |\mathbf{D}_t (\bar{\mathbf{y}}_n - \hat{\mathbf{f}}_n)| \\ &= |\mathbf{D}_t \mathbf{D}^T \hat{\mathbf{u}}| \leq 4 \lambda_n, \end{aligned}$$

which is captured in event B_n . The last inequality in the above equation occurs because, from Theorem 2, we have $|\hat{\mathbf{u}}| \leq \lambda_n$ as well as the fact that $\sum_{i=1}^m |[\mathbf{D}_t \mathbf{D}^T]_i| = 2^{r+2}$, for an arbitrary r . In the following, we derive the conditions under which the probabilities of both events A_n and B_n converge to 1.

- To compute the probability of A_n , we first note that, for every $t \in \tau$,

$$\begin{aligned}
|\mathbf{D}_t \widehat{\mathbf{f}}_n| &= |\bar{\mathbf{y}}_{n,t} - \bar{\mathbf{y}}_{n,t-1} - \lambda_n(s_t - s_{t-1})| \\
&= |\mathbf{D}_t \bar{\boldsymbol{\varepsilon}}_n + \mathbf{D}_t \mathbf{f} - \lambda_n(s_t - s_{t-1})| \\
&\leq |\mathbf{D}_t \bar{\boldsymbol{\varepsilon}}_n - \lambda_n(s_t - s_{t-1})| + |\mathbf{D}_t \mathbf{f}|,
\end{aligned}$$

where $\bar{\mathbf{y}}_{n,t}$ is the average of observations in the segment created by block t . The last inequality in the above statement is derived from the triangular inequality. Therefore, in order to verify A_n , it is enough to show that, with the probability approaching one,

$$\max_{t \in \tau} |\mathbf{D}_t \bar{\boldsymbol{\varepsilon}}_n - \lambda_n(s_t - s_{t-1})| \leq \delta_n, \quad (\text{A.8})$$

where $\delta_n = \min_{t \in \tau} |\mathbf{D}_t \mathbf{f}|$ is the minimum jump between change points. Equivalently, it suffices to show that

$$\max_{t \in \tau} \lambda_n |s_t - s_{t-1}| \leq \delta_n/2, \quad (\text{A.9})$$

and

$$\max_{t \in \tau} |\mathbf{D}_t \bar{\boldsymbol{\varepsilon}}_n| \leq \delta_n/2. \quad (\text{A.10})$$

The inequality in (A.9) holds if $\lambda_n \leq \frac{\delta_n \underline{L}_n}{4}$, where $\underline{L}_n = \min_{j=0, \dots, J_0} |\tau_{j+1} - \tau_j|$. Applying the union and Gaussian tail bounds, the probability of the complement of the event in (A.10) can be computed as

$$\begin{aligned}
\Pr\left(\max_{t \in \tau} |\mathbf{D}_t \bar{\boldsymbol{\varepsilon}}_n| \geq \delta_n/2\right) &\leq \sum_{t \in \tau} \Pr(|\mathbf{D}_t \bar{\boldsymbol{\varepsilon}}_n| \geq \delta_n/2) \\
&= \sum_{t \in \tau} \Pr\left(|Z_n| \geq \frac{\delta_n \sqrt{\underline{L}_n}}{2\sqrt{2}\sigma_n}\right) \leq 2J_0 \exp\left(-\frac{\delta_n^2 \underline{L}_n}{16\sigma_n^2}\right) \\
&= 2 \exp\left(-\frac{\delta_n^2 \underline{L}_n}{16\sigma_n^2} + \log(J_0)\right). \quad (\text{A.11})
\end{aligned}$$

The probability in (A.11) converges to zero if, for some $\xi > 0$,

$$\frac{\delta_n \sqrt{\underline{L}_n}}{\sigma_n} \rightarrow \infty \quad \text{and} \quad \frac{\delta_n \sqrt{\underline{L}_n}}{\sigma_n \sqrt{\log(J_0)}} > \sqrt{16}(1 + \xi). \quad (\text{A.12})$$

- Next, we verify conditions under which $\Pr(B_n) \rightarrow 1$. Equivalently, it is enough to

determine the conditions under which the following probability converges to zero.

$$\begin{aligned}
\Pr(B_n^c) &= \Pr\left(\max_{t \in \tau^c} |\mathbf{D}_t \bar{\boldsymbol{\varepsilon}}_n| \geq 4\lambda_n\right) \leq \sum_{t \in \tau^c} \Pr(|\mathbf{D}_t \bar{\boldsymbol{\varepsilon}}_n| \geq 4\lambda_n) \\
&= \sum_{t \in \tau^c} \Pr\left(|Z_n| \geq \frac{4\lambda_n \sqrt{\underline{L}_n}}{\sqrt{2}\sigma_n}\right) \\
&\leq 2(n - J_0) \exp\left(-\frac{4\lambda_n^2 \underline{L}_n}{\sigma_n^2}\right) \\
&= 2 \exp\left(-\frac{4\lambda_n^2 \underline{L}_n}{\sigma_n^2} + \log(n - J_0)\right). \tag{A.13}
\end{aligned}$$

The above probability converges to zero if, for some $\xi > 0$, the following conditions hold,

$$\frac{\lambda_n \sqrt{\underline{L}_n}}{\sigma_n} \rightarrow \infty \quad \text{and} \quad \frac{2\lambda_n \sqrt{\underline{L}_n}}{\sigma_n \sqrt{\log(n - J_0)}} > (1 + \xi). \tag{A.14}$$

Case arbitrary r : For the piecewise polynomial of order r ($r \in \mathbb{N}$), we note that, for any $t \in [\tau_j, \tau_{j+1})$,

$$\begin{aligned}
|\mathbf{D}_t \hat{\mathbf{f}}_n| &= |\mathbf{D}_t (\mathbf{y}_n - \mathbf{D}_{-A}^T \hat{\mathbf{u}})| \\
&= \left| \mathbf{D}_t \left[(\mathbf{I} - \mathbf{P}_D) \mathbf{y}_n - \lambda_n \mathbf{P}_D \left(\mathbf{D}_{A_{j+1}}^T \mathbf{s}_{j+1} + \mathbf{D}_{A_j}^T \mathbf{s}_j \right) \right] \right| \\
&= \left| \mathbf{D}_t \left[(\mathbf{I} - \mathbf{P}_D) (\mathbf{f} + \boldsymbol{\varepsilon}_n) - \lambda_n \mathbf{P}_D \left(\mathbf{D}_{A_{j+1}}^T \mathbf{s}_{j+1} + \mathbf{D}_{A_j}^T \mathbf{s}_j \right) \right] \right|,
\end{aligned}$$

where $\mathbf{P}_D = \mathbf{D}_{-A}^T (\mathbf{D}_{-A} \mathbf{D}_{-A}^T)^{-1} \mathbf{D}_{-A}$ is the projection map onto the row space of \mathbf{D}_{-A} . In the preceding statement, the second equality is derived by plugging in the statement in (21) in place of $\hat{\mathbf{u}}$. From (19), recall that $\mathbf{I} - \mathbf{P}_D$ is equivalent to the prediction matrix in the r -th polynomial regression of \mathbf{y} onto indices $\tau_j + 1, \tau_j + 1, \dots, \tau_{j+1}$. This fact allows us to derive an upper bound for the variance of $\mathbf{D}_t (\mathbf{I} - \mathbf{P}_D) \boldsymbol{\varepsilon}_n$ (Yu and Chatterjee, 2020),

$$\max_{t \in \tau} \text{Var}\left(\mathbf{D}_t (\mathbf{I} - \mathbf{P}_D) \boldsymbol{\varepsilon}_n\right) \leq 2^{r+1} \frac{n^{2r} \sigma_n^2}{\underline{L}_n^{2r+1}}.$$

Following a procedure similar to that used in the case $r = 0$,

$$\Pr\left(\max_{t \in \tau} |\mathbf{D}_t (\mathbf{I} - \mathbf{P}_D) \boldsymbol{\varepsilon}_n| \geq \frac{\delta_n}{2}\right) \leq 2 \exp\left(-\frac{\delta_n^2 \underline{L}_n^{2r+1}}{2^{r+4} n^{2r} \sigma_n^2} + \log(J_0)\right). \tag{A.15}$$

For the case of an arbitrary r , there is a slight modification in the definition of event B_n :

$$B_n = \left\{ \max_{t \in \tau^c} |\mathbf{D}_t (\mathbf{I} - \mathbf{P}_D) \boldsymbol{\varepsilon}_n| \leq 2^{r+2} \lambda_n \right\}. \tag{A.16}$$

Again, in the same manner

$$\Pr(B_n^c) \leq 2 \exp\left(-\frac{2^{r+2} \lambda_n^2 \underline{L}_n^{2r+1}}{n^{2r} \sigma_n^2} + \log(n - J_0)\right). \tag{A.17}$$

Therefore, for an arbitrary r , the PRUTF algorithm is consistent in pattern recovery if, in addition to

$$\lambda_n < \frac{\delta_n \underline{L}_n^{2r+1}}{n^{2r} 2^{r+2}},$$

the conditions in (42) and (43) hold.

- (b) As shown in part (c) of Theorem 2, in staircase blocks, the violation of the KKT conditions boils down to crossing the zero line for a Gaussian bridge process. Suppose j -th block is a staircase block; therefore, PRUTF can attain the exact discovery if $\hat{u}_j^{\text{st}}(t) \leq 0$ or $\hat{u}_j^{\text{st}}(t) \geq 0$, for all $(\tau_j + r_a)/m \leq t \leq (\tau_{j+1} - r_b)/m$. Hence the probability of this event occurring is equal to $\Pr\left(\max_{0 \leq t \leq L_j} \hat{u}_j^{\text{st}}(t) \leq 0\right)$. According to [Beghin and Orsingher \(1999\)](#),

$$\Pr\left(\max_{0 \leq t \leq L_j} \hat{u}_j^{\text{st}}(t) \leq a\right) = 1 - \exp\left(-\frac{2a^2}{S_r^2(L_j)}\right), \quad (\text{A.18})$$

where $S_r^2(L_j)$ is the L_j -th diagonal element of the matrix $\sigma^2(\mathbf{D}_{A_j} \mathbf{D}_{A_j}^T)^{-1}$. As a result, the probability converges to zero as a vanishes. This result implies that the PRUTF algorithm fails to consistently recover the true pattern in the presence of staircase patterns.

Bibliography

- Adler, R. J. and Taylor, J. E. (2009). *Random fields and geometry*. Springer.
- Ali, A., Tibshirani, R. J., et al. (2019). The generalized lasso problem and uniqueness. *Electronic Journal of Statistics*, 13(2):2307–2347.
- Aminikhanghahi, S. and Cook, D. J. (2017). A survey of methods for time series change point detection. *Knowledge and Information Systems*, 51(2):339–367.
- Anastasiou, A. and Fryzlewicz, P. (2019). Detecting multiple generalized change-points by isolating single ones. *arXiv preprint arXiv:1901.10852*.
- Arnold, T. B. and Tibshirani, R. J. (2016). Efficient implementations of the generalized lasso dual path algorithm. *Journal of Computational and Graphical Statistics*, 25(1):1–27.
- Auger, I. E. and Lawrence, C. E. (1989). Algorithms for the optimal identification of segment neighborhoods. *Bulletin of mathematical biology*, 51(1):39–54.
- Bai, J. (1997). Estimating multiple breaks one at a time. *Econometric theory*, 13(3):315–352.
- Bai, J. and Perron, P. (2003). Computation and analysis of multiple structural change models. *Journal of applied econometrics*, 18(1):1–22.
- Baranowski, R., Chen, Y., and Fryzlewicz, P. (2019). Narrowest-over-threshold detection of multiple change points and change-point-like features. *Journal of the Royal Statistical Society: Series B (Statistical Methodology)*, 81(3):649–672.
- Beghin, L. and Orsingher, E. (1999). On the maximum of the generalized brownian bridge. *Lithuanian Mathematical Journal*, 39(2):157–167.
- Bianchi, M., Boyle, M., and Hollingsworth, D. (1999). A comparison of methods for trend estimation. *Applied Economics Letters*, 6(2):103–109.
- Billingsley, P. (2013). *Convergence of probability measures*. John Wiley and Sons.
- Boyd, S., Parikh, N., Chu, E., Peleato, B., Eckstein, J., et al. (2011). Distributed optimization and statistical learning via the alternating direction method of multipliers. *Foundations and Trends® in Machine learning*, 3(1):1–122.
- Boyd, S. and Vandenberghe, L. (2004). *Convex optimization*. Cambridge university press.
- Brezis, H. (2010). *Functional analysis, Sobolev spaces and partial differential equations*. Springer Science & Business Media.
- Ciuperca, G. (2011). A general criterion to determine the number of change-points. *Statistics & Probability Letters*, 81(8):1267–1275.
- Ciuperca, G. (2014). Model selection by lasso methods in a change-point model. *Statistical Papers*, 55(2):349–374.

- Demetriou, I. and Lipitakis, E. (2001). Certain positive definite submatrices that arise from binomial coefficient matrices. *Applied numerical mathematics*, 36(2-3):219–229.
- Donsker, M. D. (1951). *An invariance principle for certain probability limit theorems*.
- Eckley, I. A., Fearnhead, P., and Killick, R. (2011). Analysis of changepoint models. *Bayesian Time Series Models*, pages 205–224.
- Frick, K., Munk, A., and Sieling, H. (2014). Multiscale change point inference. *Journal of the Royal Statistical Society: Series B (Statistical Methodology)*, 76(3):495–580.
- Fryzlewicz, P. (2018). Detecting possibly frequent change-points: Wild binary segmentation 2 and steepest-drop model selection. *arXiv preprint arXiv:1812.06880*.
- Fryzlewicz, P. et al. (2014). Wild binary segmentation for multiple change-point detection. *The Annals of Statistics*, 42(6):2243–2281.
- Fryzlewicz, P. et al. (2018). Tail-greedy bottom-up data decompositions and fast multiple change-point detection. *The Annals of Statistics*, 46(6B):3390–3421.
- Futschik, A., Hotz, T., Munk, A., and Sieling, H. (2014). Multiscale dna partitioning: statistical evidence for segments. *Bioinformatics*, 30(16):2255–2262.
- Galceran, E., Cunningham, A. G., Eustice, R. M., and Olson, E. (2017). Multipolicy decision-making for autonomous driving via changepoint-based behavior prediction: Theory and experiment. *Autonomous Robots*, 41(6):1367–1382.
- Gasbarra, D., Sottinen, T., and Valkeila, E. (2007). Gaussian bridges. In *Stochastic analysis and applications*, pages 361–382. Springer.
- Green, P. J. and Silverman, B. W. (1993). *Nonparametric regression and generalized linear models: a roughness penalty approach*. Chapman and Hall/CRC.
- Hampel, F. R. (1974). The influence curve and its role in robust estimation. *Journal of the American Statistical Association*, 69(346):383–393.
- Hansen, B. E. (2001). The new econometrics of structural change: dating breaks in us labour productivity. *Journal of Economic perspectives*, 15(4):117–128.
- Hansen, J., Ruedy, R., Sato, M., and Lo, K. (2010). Global surface temperature change. *Reviews of Geophysics*, 48(4).
- Harchaoui, Z. and Lévy-Leduc, C. (2010). Multiple change-point estimation with a total variation penalty. *Journal of the American Statistical Association*, 105(492):1480–1493.
- Horváth, L. and Rice, G. (2014). Extensions of some classical methods in change point analysis. *Test*, 23(2):219–255.

- Hoskins, W. and Ponzo, P. (1972). Some properties of a class of band matrices. *Mathematics of Computation*, 26(118):393–400.
- Huang, T., Wu, B., Lizardi, P., and Zhao, H. (2005). Detection of dna copy number alterations using penalized least squares regression. *Bioinformatics*, 21(20):3811–3817.
- Jackson, B., Scargle, J. D., Barnes, D., Arabhi, S., Alt, A., Gioumoussis, P., Gwin, E., Sangtrakulcharoen, P., Tan, L., and Tsai, T. T. (2005). An algorithm for optimal partitioning of data on an interval. *IEEE Signal Processing Letters*, 12(2):105–108.
- James, N. A. and Matteson, D. S. (2015). Change points via probabilistically pruned objectives. *arXiv preprint arXiv:1505.04302*.
- Jia, J., Rohe, K., et al. (2015). Preconditioning the lasso for sign consistency. *Electronic Journal of Statistics*, 9(1):1150–1172.
- Killick, R., Fearnhead, P., and Eckley, I. A. (2012). Optimal detection of changepoints with a linear computational cost. *Journal of the American Statistical Association*, 107(500):1590–1598.
- Kim, S.-J., Koh, K., Boyd, S., and Gorinevsky, D. (2009). ℓ_1 trend filtering. *SIAM review*, 51(2):339–360.
- Lavielle, M. (2005). Using penalized contrasts for the change-point problem. *Signal processing*, 85(8):1501–1510.
- Lee, T.-S. (2010). Change-point problems: bibliography and review. *Journal of Statistical Theory and Practice*, 4(4):643–662.
- Lenssen, N. J., Schmidt, G. A., Hansen, J. E., Menne, M. J., Persin, A., Ruedy, R., and Zyss, D. (2019). Improvements in the uncertainty model in the goddard institute for space studies surface temperature (gistemp) analysis. *Journal of Geophysical Research: Atmospheres*.
- Liu, D., Chen, X., Lian, Y., and Lou, Z. (2010). Impacts of climate change and human activities on surface runoff in the dongjiang river basin of china. *Hydrological Processes: An International Journal*, 24(11):1487–1495.
- Lung-Yut-Fong, A., Lévy-Leduc, C., and Cappé, O. (2012). Distributed detection/localization of change-points in high-dimensional network traffic data. *Statistics and Computing*, 22(2):485–496.
- Maidstone, R., Hocking, T., Rigaiil, G., and Fearnhead, P. (2017). On optimal multiple change-point algorithms for large data. *Statistics and Computing*, 27(2):519–533.
- Mairal, J. and Yu, B. (2012). Complexity analysis of the lasso regularization path. *arXiv preprint arXiv:1205.0079*.
- Mammen, E., van de Geer, S., et al. (1997). Locally adaptive regression splines. *The Annals of Statistics*, 25(1):387–413.

- Olshen, A. B., Venkatraman, E., Lucito, R., and Wigler, M. (2004). Circular binary segmentation for the analysis of array-based dna copy number data. *Biostatistics*, 5(4):557–572.
- Osborne, M. R., Presnell, B., and Turlach, B. A. (2000). On the lasso and its dual. *Journal of Computational and Graphical statistics*, 9(2):319–337.
- Oudre, L., Lung-Yut-Fong, A., and Bianchi, P. (2011). Segmentation of accelerometer signals recorded during continuous treadmill walking. In *2011 19th European Signal Processing Conference*, pages 1564–1568. IEEE.
- Page, E. (1955). A test for a change in a parameter occurring at an unknown point. *Biometrika*, 42(3/4):523–527.
- Page, E. S. (1954). Continuous inspection schemes. *Biometrika*, 41(1/2):100–115.
- Pan, J. and Chen, J. (2006). Application of modified information criterion to multiple change point problems. *Journal of multivariate analysis*, 97(10):2221–2241.
- Pezzatti, G. B., Zumbrunnen, T., Bürgi, M., Ambrosetti, P., and Conedera, M. (2013). Fire regime shifts as a consequence of fire policy and socio-economic development: an analysis based on the change point approach. *Forest Policy and Economics*, 29:7–18.
- Qian, J. and Jia, J. (2016). On stepwise pattern recovery of the fused lasso. *Computational Statistics & Data Analysis*, 94:221–237.
- Ramdas, A. and Tibshirani, R. J. (2016). Fast and flexible admm algorithms for trend filtering. *Journal of Computational and Graphical Statistics*, 25(3):839–858.
- Ranganathan, A. (2012). Pliss: labeling places using online changepoint detection. *Autonomous Robots*, 32(4):351–368.
- Rigaiil, G. (2015). A pruned dynamic programming algorithm to recover the best segmentations with 1 to k_max change-points. *Journal de la Société Française de Statistique*, 156(4):180–205.
- Rinaldo, A. (2014). Corrections to properties and refinements of the fused lasso.
- Rinaldo, A. et al. (2009). Properties and refinements of the fused lasso. *The Annals of Statistics*, 37(5B):2922–2952.
- Robbins, M. W., Lund, R. B., Gallagher, C. M., and Lu, Q. (2011). Changepoints in the north atlantic tropical cyclone record. *Journal of the American Statistical Association*, 106(493):89–99.
- Rojas, C. R. and Wahlberg, B. (2014). On change point detection using the fused lasso method. *arXiv preprint arXiv:1401.5408*.
- Ruggieri, E. (2013). A bayesian approach to detecting change points in climatic records. *International Journal of Climatology*, 33(2):520–528.

- Shorack, G. R. and Wellner, J. A. (2009). *Empirical processes with applications to statistics*. SIAM.
- Siris, V. A. and Papagalou, F. (2004). Application of anomaly detection algorithms for detecting syn flooding attacks. In *IEEE Global Telecommunications Conference, 2004. GLOBE-COM'04.*, volume 4, pages 2050–2054. IEEE.
- Stasinopoulos, D. and Rigby, R. (1992). Detecting break points in generalised linear models. *Computational Statistics & Data Analysis*, 13(4):461–471.
- Steidl, G., Didas, S., and Neumann, J. (2006). Splines in higher order tv regularization. *International journal of computer vision*, 70(3):241–255.
- Tibshirani, R. (1996). Regression shrinkage and selection via the lasso. *Journal of the Royal Statistical Society: Series B (Methodological)*, 58(1):267–288.
- Tibshirani, R. J. (2011). *The solution path of the generalized lasso*. Stanford University.
- Tibshirani, R. J. et al. (2013). The lasso problem and uniqueness. *Electronic Journal of Statistics*, 7:1456–1490.
- Tibshirani, R. J. et al. (2014). Adaptive piecewise polynomial estimation via trend filtering. *The Annals of Statistics*, 42(1):285–323.
- Truong, C., Oudre, L., and Vayatis, N. (2018). A review of change point detection methods. *arXiv preprint arXiv:1801.00718*.
- Van Der Vaart, A. and Wellner, J. (1996). Weak convergence and empirical processes: With applications to statistics springer series in statistics. *Springer*, 58:59.
- Vostrikova, L. Y. (1981). Detecting "disorder" in multidimensional random processes. In *Doklady Akademii Nauk*, volume 259, pages 270–274. Russian Academy of Sciences.
- Wainwright, M. J. (2009). Sharp thresholds for high-dimensional and noisy sparsity recovery using ℓ_1 -constrained quadratic programming (lasso). *IEEE transactions on information theory*, 55(5):2183–2202.
- Wang, D., Yu, Y., Rinaldo, A., et al. (2020). Univariate mean change point detection: Penalization, cusum and optimality. *Electronic Journal of Statistics*, 14(1):1917–1961.
- Wang, Y.-X., Smola, A., and Tibshirani, R. (2014). The falling factorial basis and its statistical applications. In *International Conference on Machine Learning*, pages 730–738.
- Wu, Y. (2008). Simultaneous change point analysis and variable selection in a regression problem. *Journal of Multivariate Analysis*, 99(9):2154–2171.
- Yao, Y.-C. (1988). Estimating the number of change-points via schwarz'criterion. *Statistics & Probability Letters*, 6(3):181–189.

- Yao, Y.-C. and Au, S.-T. (1989). Least-squares estimation of a step function. *Sankhyā: The Indian Journal of Statistics, Series A*, pages 370–381.
- Yu, Y. and Chatterjee, S. (2020). Localising change points in piecewise polynomials of general degrees. *arXiv preprint arXiv:2007.09910*.
- Zhang, N. R. and Siegmund, D. O. (2007). A modified bayes information criterion with applications to the analysis of comparative genomic hybridization data. *Biometrics*, 63(1):22–32.
- Zhao, P. and Yu, B. (2006). On model selection consistency of lasso. *Journal of Machine learning research*, 7(Nov):2541–2563.